The Journal of Physical Chemistry A

 VOLUME 101, NUMBER 47, NOVEMBER 20, 1997

ARTICLES

Ultrafast X-ray and Electron Diffraction: Theoretical Considerations

M. Ben-Nun,† Jianshu Cao, and Kent R. Wilson*

Department of Chemistry and Biochemistry, University of California San Diego, La Jolla, California 92093-0339

Received: May 30, 1997; In Final Form: August 27, 1997[⊗]

Time-dependent ultrafast diffraction measurements can be directly inverted to obtain the dynamics of atomic motions, in contrast to ultrafast spectra which require detailed knowledge of the sample (e.g., potential energy surfaces) for their inversion. We consider here how to derive time-dependent diffraction (the X-ray and electron diffraction cases being very similar) from nuclear quantum dynamics and vice versa and how this may be used to directly observe the atomic motions in molecules, in particular how chemical reactions take place. Two simple examples of dissociative and bound quantum (vibrational and rotational) dynamics in a gas-phase sample of diatomic molecules, excited by an optical pump pulse and measured by an electron or X-ray probe pulse, are presented. The quantum mechanical basis of the breaking of symmetry due to the linearly polarized optical pump pulse and the superposition and interference between the ground and excited electronic states are discussed. We demonstrate how to isolate the short-time excited-state dynamics from that of the ground state using the symmetry of the electronic dipole transition. We illustrate that the time-evolving distribution of interatomic distances can be clearly resolved from the ultrafast diffraction data and thus illustrate that the detailed dynamics of molecular vibration and the progress of a photodissociation reaction could be watched as they occur. In addition, we show that the duration of ultrafast X-ray and electron pulses can be measured with a time resolution of tens of femtoseconds by clocking it against such atomic motion.

I. Introduction

X-ray and in many cases electron diffraction have been used to resolve the electron density and equilibrium structure of a large number of small molecules as well as of many important biomolecules and biopolymers.[1−5] Our knowledge of time-evolving structures, on the other hand, is much more limited and it is mainly due to optical pump−probe experiments,[6] which can now be carried out with a routine resolution of tens of femtoseconds. Although the time resolution in these optical experiments allows in principle a detailed observation of atomic motions, more often than not it is impossible to "invert" the measurements to the desired positions of the atoms because the connection between the atomic positions and the experimental observable requires knowledge of such properties as the potential energy surfaces as well as polarizabilities (nonresonance Raman), dipole moments (infrared), and transition dipole moments (electronic absorption and resonance Raman). Unlike this rather complicated (and often unknown) relation between the experimental observable and the interatomic distances for optical probe experiments, the connection between the atomic positions and the scattering (X-ray or electron) amplitude is clear and well-known: the two are linked by a Fourier relation.[1−5] In addition, the theoretical treatments of electron and X-ray diffraction are very similar. With this in mind, it has been proposed (see refs 7−9 for a recent review and collections of papers) that ultrafast time-resolved X-ray and electron diffraction may be used to directly watch structural changes and atomic motions during chemical (and biochemical) reactions and/or physical changes (such as phase transitions).

Conceptually, the method is similar to an ultrafast optical pump−probe experiment. The essential new ingredient is that the probing is not optical but is via X-ray or electron diffraction. This combines the direct inversion advantages of X-ray and electron techniques (the experimental measurements are done in momentum, **k**, space and are inverted to real, **r**, space) with the high temporal resolution of ultrafast optical pump−probe techniques. In an optical pump−diffraction probe experiment, the dynamics is initiated by an ultrafast light pulse and then

† Present address: Department of Chemistry, University of Illinois, Urbana, IL 61801.

[⊗] Abstract published in *Advance ACS Abstracts*, October 15, 1997.

S1089-5639(97)01764-7 CCC: $14.00

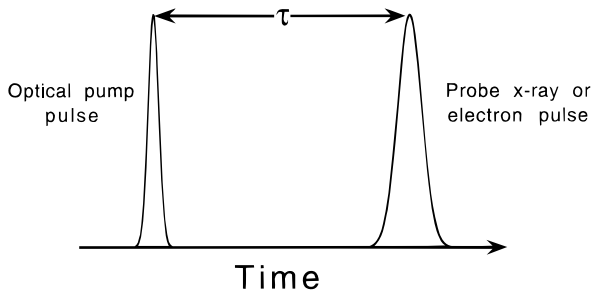

Figure 1. An illustration of the optical pump−diffraction probe (X-ray or electron) experimental scheme. An ultrafast optical pulse initiates a chemical reaction, or other time-dependent process, and at various increasing delay times, τ, the system is probed with a short X-ray or electron pulse.

probed (at various increasing delay times) by ultrafast diffraction (X-ray or electron), as shown in Figure 1. By taking "snapshots" of the atomic positions as a function of delay time after the reaction is initiated by a pulse of light, and stringing them together as frames in a "movie", one can watch the dynamics as the structures of molecules evolve in time, for example, during the course of a chemical reaction.

Although the idea of ultrafast time-resolved diffraction experiments is appealing, it is experimentally very challenging because the X-ray or electron source must satisfy particular requirements concerning pulse duration, synchronization with the optical pump pulse, energy width, brightness, and flux. In addition, for electron pulses, special attention must be paid to the effect of repulsion between the electrons and of the difference in electron and photon velocities.[10] In the next few paragraphs, we discuss some of the experimental and theoretical studies on ultrashort X-ray and electron diffraction. In each case (X-ray and electron), we first discuss the experimental work and then proceed with the theoretical one. We begin with fast X-ray diffraction.

Various sources have been used to generate ultrafast X-ray pulses. The early work (beginning in the late 1960s) on time-resolved X-ray diffraction was based on electron impact sources.[11−14] More recently, picosecond X-ray pulse time scales were achieved using vacuum X-ray diodes with a laser-triggered photocathode.[15−24] Laser-produced plasma X-ray sources offer exceptionally short X-ray pulses whose duration has been systematically reduced from the nanosecond range to the subpicosecond range.[25−40] As recently demonstrated in a pulsed Laue X-ray protein crystal diffraction experiment,[41] with a nanosecond time resolution, synchrotrons provide exceptionally bright X-ray sources that can produce X-ray pulses of 40−100 ps.[42] (For a recent collection of papers on time-resolved macromolecular crystallography, see ref 43.) Finally, the best X-ray pulse temporal resolution (300 fs) has been achieved by utilizing Thomson scattering of optical photons from a relativistic electron beam.[44−46]

Relatively, few theoretical studies have discussed the use of ultrafast X-ray pulses as a tool for studying ultrafast molecular dynamics. The first theoretical treatment of molecular dynamics and ultrafast diffraction, by Wilson and co-workers,[15,16] used classical MD simulations to compute the diffraction resulting from I_2 photodissociation in the gas phase and from the subsequent caging and possible recombination in various solvents. More recently, Lin et al.[47] discussed the theory of ultrafast time-resolved X-ray diffraction and applied their theory to the vaporization kinetics of finite systems. Recently, we have discussed some theoretical aspects of ultrafast X-ray absorption and diffraction[48] and, in addition, have theoretically illustrated that the change in electron density distribution upon electronic excitation of atoms can significantly change their X-ray and electron diffraction intensities,[49] suggesting that electronic structures of excited electronic states may be directly observed using optical pump−diffraction probe techniques.

Although gas-phase X-ray diffraction was demonstrated in 1929 when Debye and co-workers imaged the scattering pattern of carbon tetrachloride vapor,[50] it is more common to use electrons for gas-phase samples in order to overcome the problem of the low-scattering cross section for hard X-rays. The first gas-phase experiments with a pulsed electron beam synchronous with photoexcitation were performed by Ischenko et al.[51,52] and Rood and Milledge.[53] Nanosecond electron pulses, produced by light-stimulated emission,[54−57] have been used to study structural kinetics in various photoexcitation processes. Zewail and co-workers have studied the effect of UV photodissociation[58,59] on electron diffraction intensities using femtosecond optical pulses for the photoexcitation process and picosecond range electron pulses for the probing process. Stroboscopic electron diffraction has not been limited to the gas phase. Laser-induced melting of films and laser-induced transient temperature changes in a single crystal have been directly observed using picosecond range electron pulses.[60−67] A comprehensive review on recent developments in time-resolved surface electron diffraction studies can be found in ref 68.

From a theoretical point of view, Williamson and Zewail have discussed aspects of the experimental methodology of ultrafast gas-phase electron diffraction[69] and in particular the problem of velocity mismatch and temporal resolution in crossed-beam experiments.[10] The effect of spatial alignment induced by the polarization of the optical pump pulse has been discussed both by Williamson and Zewail[70] and by Ischenko et al.[57] (In both studies only one potential surface was considered.) Ewbank et al.[56] have also discussed in detail the inversion of the scattering intensities to real space and the computation of potential energy surfaces for the case of a diatomic molecule. Finally, a stochastic approach to structural and vibrational kinetics that can be used to model time-resolved gas-phase electron diffraction has also been presented by Ischenko et al.[71−73]

Although the experimental scheme that we discuss in this paper is a direct extension of stationary diffraction experiments, it poses new theoretical questions because the pump pulse, the sample, and the probe pulse are all time-dependent.[48] If, as discussed in this paper, the molecular dynamics is initiated by an ultrashort optical pulse, then the probe pulse scatters from a sample that consists of an initially coherent superposition of rotational, vibrational, and electronic states. The presence of more than one electronic state in the sample implies that one cannot restrict attention to the nuclear dynamics of a single state but may have to consider the dynamics of multiple electronic states. This can lead to interference among states, as discussed in this paper. This problem is not unique to optical pump−diffraction probe experiments and it is encountered in any modeling of a photochemical reaction where the interesting dynamics begins on an electronically excited state. The multi-electronic-state problem is, however, more severe for optical pump−diffraction probe experiments. Unlike optical probing that is usually electronic-state specific, X-ray and electron probing has the disadvantage of being insensitive to electronic-state labeling (in other words, all electronic states contribute to the diffraction pattern). To properly treat and understand the coherence and interference among states, both the nuclear and electronic degrees of freedom need to be considered quantum mechanically. Later, after the quantum effects are understood, appropriate approximations can be made. Exact quantum

mechanical computations cannot be performed for large polyatomic systems (and/or condensed phases) and other, computationally less demanding, methods will have to be invoked to model such systems.[74,75]

As in previous time-dependent diffraction studies, we, in this paper, also limit our discussion to the nuclear dynamics and ignore the electron dynamics.[49] Our derivation approximates the electron density by a sum of nonoverlapping densities (each of which is localized about the instantaneous position of an atom in the molecule), and thus, it cannot account for the deformation of the electron density during the course of reaction. Within this approximation, the time dependence of the diffraction intensities that we compute and discuss is associated only with the nuclear motion, and bonding changes in valence electrons are ignored. This approximation is sufficient at this time because the current accuracy (as well as signal-to-noise ratio) of pulsed electron and X-ray experiments is insufficient to resolve the scattering of a few bonding electrons from that of the dominant core electrons. Elsewhere, we have discussed the changes in diffraction given by valence electron excitation which may in time be resolved in ultrafast experiments.[49]

The general theory for ultrafast optical pump−diffraction (X-ray or electron) probe experiments is presented in section II.A. This general derivation (for both X-ray and electron diffraction) is followed by a more specific discussion of X-ray diffraction for a two-electronic-state diatomic molecule, section II.B. Two simple numerical examples are presented in section III: the ultrafast photodissociation of molecular bromine and the bound vibrational motion in electronically excited iodine. We point out that such molecular motions can be used as a clock to measure the duration of X-ray and electron pulses with tens of femtoseconds time resolution. In section IV we discuss the inversion of the data from momentum space, **k**, to coordinate space, **r**. In both sections III and IV, special attention is given to the previously discussed[15,16,57,70] breaking of symmetry in the sample due to the linearly polarized optical pump pulse (electrostatic hexapole techniques[76,77] have also been used to demonstrate symmetry breaking in diffraction from gas-phase samples). In section IV we use the symmetry of the electronic dipole transition in order to isolate the excited-state dynamics from that of the ground state. Many technical details regarding the computation of the angular part of the molecular wave function (and the scattering integrals) are summarized in the Appendix. As discussed in section III and in the Appendix, our treatment of the nuclear wave functions is only approximate: the three-dimensional two-electronic-state wave function is written as a product of an angular independent radial part and an angular part. The radial part is computed numerically, by propagating the two-electronic state one-dimensional Schrödinger equation, and the angular part is evaluated analytically assuming a single photon process for the excited state and a two photon process for the ground state.

II. Theory

In this section the theoretical treatments of gas-phase X-ray and electron diffraction (which are quite similar) are discussed for the case when more then one electronic state contributes to the measured scattering intensity. The general theory (for both X-ray and electron diffraction) is presented in section II.A, and it is followed by a more specific discussion of a two-electronic-state diatomic molecule in section II.B. Like previous derivations of stationary[4,78] and time-dependent X-ray and electron diffraction theories,[15,16,54,56−59,70] we assume that the scattering process is elastic with respect to the electronic degrees of freedom and inelastic with respect to the (rotational and vibrational) nuclear degrees of freedom. Hence, the scattering (amplitude and) intensity is first evaluated for a fixed nuclear configuration and then averaged over the nuclear degrees of freedom (i.e., vibrations and rotations). However, we do differ from all previous time-dependent studies in that (i) we explicitly compute the optical excitation stage and do take into account the resulting mixture of ground and excited electronic states. (ii) We treat the resulting coherent superposition of rovibrational states quantum mechanically, and (iii) we pay special attention to the coherence length and pulse duration of the probe X-ray or electron pulse. As will be shown in section II.B these considerations imply that for a multi-electronic-state system the instantaneous X-ray (and electron) scattering intensity (eq 2.12) is not given by the sum of the individual electronic-state scattering intensities. It has cross terms that are a product of scattering amplitudes from different electronic states. However, these cross terms can only be observed if the duration of the probe X-ray or electron pulse is approximately of the order of, or shorter than, the oscillation period of these terms (eq 2.16, 2.15).

A. General Derivation of Time-Dependent X-ray and Electron Diffraction Theory. Our derivation begins with a short summary of conventional (i.e., time-independent) X-ray and electron diffraction theory, whose theoretical principles are similar and very well established: X-ray photons (away from specific resonances) are solely scattered by the electronic charge density cloud whereas electrons have an additional scattering term that is due to the nuclear charge density. In this paper, we consider only scattering using the first Born approximation[79] (i.e., first-order perturbation theory) and ignore the effect of any absorption processes. This approximation is very reasonable for the examples shown, and for wavelengths that are far from any absorption edge.[78] Within the first Born approximation [and the independent atom model (IAM)[4,78] see below], the elastic X-ray scattering intensity of rigid centers moving according to quantum dynamics of the nuclei on a single Born−Oppenheimer potential energy surface is given by

$$I_x(\mathbf{s}) = \langle \chi^\nu(\mathbf{R}) | \sum_{\alpha,\beta}^{N} f(\mathbf{s})^{\alpha *} f(\mathbf{s})^{\beta} \exp[i\mathbf{s}\cdot(\mathbf{R}_\beta - \mathbf{R}_\alpha)] | \chi^\nu(\mathbf{R}) \rangle \quad (2.1)$$

In eq 2.1 the following standard definitions have been used. First, the total wave function, $\psi(\mathbf{r}, \mathbf{R})$, was written as a product of an electronic wave function, $\phi(\mathbf{r}; \mathbf{R})$, with the usual parametric dependence on the nuclear coordinates **R**, and a rovibrational nuclear eigenfunction, $\chi^\nu(\mathbf{R})$: $\psi(\mathbf{r},\mathbf{R}) = \phi(\mathbf{r};\mathbf{R})\chi^V(\mathbf{R})$. In what follows, we use Greek letters for nuclear indices. Next, the exact electronic wave function, $\phi(\mathbf{r}; \mathbf{R})$, was approximated by a sum of nonoverlapping electronic wave functions (the IAM[4,78]), each of which is localized about the position of an atom in the molecule:

$$\phi(\mathbf{r}; \mathbf{R}) \approx \sum_{\alpha=1}^{N} \varphi^\alpha(\mathbf{r}_\alpha = \mathbf{r} - \mathbf{R}_\alpha; \mathbf{R}_\alpha) \quad (2.2)$$

The summation in eq 2.2 (and eq 2.1) extends over all *N* atoms in the molecule, and we used a set of electronic coordinates, $\mathbf{r}_\alpha$, that refers to the nuclear positions, $\mathbf{R}_\alpha$, as the origin. Within the IAM approximation, $f^\alpha(\mathbf{s})$ is the scattering amplitude of atom α

$$f^\alpha(\mathbf{s}) \equiv f^\alpha = \int d\mathbf{r}_\alpha \varphi^{\alpha *} \exp(i\mathbf{s}\cdot\mathbf{r}_\alpha)\varphi^\alpha \quad (2.3)$$

in which **s** is the difference between the incident, $\mathbf{k}_o$, and scattered, **k**, wave vectors,

$$\mathbf{s} = \mathbf{k}_o - \mathbf{k} \tag{2.4}$$

As noted above, electrons scatter from the total charge density (electronic plus nuclear), $\rho_e + \rho_n$, in which ρ_e is the electronic density and ρ_n is the nuclear charge density, the latter taken here as a δ function.[80] There is thus an additional "nuclear" term which is due to the scattering of the electrons from the αth nucleus with charge Z_α, and within the IAM and first Born approximation the elastic electron scattering amplitude of atom α is given by[81]

$$g^\alpha(\mathbf{s}) \equiv g^\alpha = \frac{1}{s^2}[Z_\alpha - f^\alpha(\mathbf{s})] \tag{2.5}$$

Using eq 2.5, the electron scattering intensity is derived by replacing the X-ray operator (f^α) with the electron operator (g^α). Finally, since in general the system is initially in vibrational and rotational equilibrium, the scattering intensity (X-ray and/or electron) needs to be averaged over a ro-vibrational Boltzmann distribution (at the appropriate temperature).

We now discuss the scattering amplitudes, and subsequently intensities, for the case of a sample that is driven synchronously by an ultrafast coherent optical pump pulse and then probed (at various delay times with respect to the optical pump pulse) by an ultrafast X-ray or electron pulse. After an interaction with coherent laser light, the total molecular wave function is given by a linear combination of product wave functions, each one being taken as a Born−Oppenheimer product of an electronic part, $\phi_j(\mathbf{r}; \mathbf{R})$, and an associated time-dependent nuclear part, $\chi_j(\mathbf{R}, t)$,[82]

$$\Psi(\mathbf{r}, \mathbf{R}, t) = \sum_j C_j(t)\phi_j(\mathbf{r}; \mathbf{R})\chi_j(\mathbf{R}, t) = \sum_j C_j(t)\phi_j(\mathbf{r}; \mathbf{R})\sum_\nu d_j^\nu(t)\chi_j^\nu(\mathbf{R}) \tag{2.6}$$

In eq 2.6, the IAM has not yet been invoked, and thus $\phi_j(\mathbf{r}; \mathbf{R})$ is the exact jth orthonormal electronic eigenfunction. $\chi_j^\nu(\mathbf{R})$ is the νth ro-vibrational nuclear eigenfunction on the jth electronic surface [with a time-dependent coefficient $d_j^\nu(t)$], the index ν implying a summation over all nuclear indices, i.e., vibrational and rotational. Both the nuclear and the electronic wave functions are normalized to unity so that $|C_j(t)|^2$ is the time-dependent (fractional, i.e., $\sum_j n_j(t) = 1$), population of the jth electronic state. [Note that $\Psi(\mathbf{r}, \mathbf{R}, t)$ is an M dimensional vector, where M is the number of electronic states and that the use of a time-dependent nuclear wave packet is dictated by the nature of the optical excitation by the pump pulse that results in a nonstationary nuclear wave function.[82]]

Using this multi-electronic-state wave function we next want to evaluate the scattering amplitude and intensity. Before doing, so we need to discuss the properties of the ultrafast probe pulse. Consider, for example, laser-produced plasma X-ray sources. These sources produce pulses that can be considered as an incoherent sum of many ultrashort subpulses. The duration of each of these ultrashort subpulses is determined by the (femtosecond) lifetime of the atomic hole state that emitted the X-ray photon. The computation of the scattering intensity will therefore be divided into two parts. We first compute the instantaneous scattering amplitude and intensity (eqs 2.9−2.12). This amplitude and/or intensity corresponds to the scattering of a single X-ray photon (or electron) from a coherent multi-electronic-state sample. Second, the total X-ray or electron scattering intensity is evaluated by a weighted summation of the instantaneous scattering intensities (integrated over the nuclear ro-vibrational degrees of freedom), with the weights given by the temporal profile of the X-ray or electron field intensity (eqs 2.13−2.16).

Given eq 2.6 for the multi-electronic-state wave function, and the above discussion of the properties of the X-ray probe pulse, the instantaneous X-ray scattering amplitude (for a fixed nuclear configuration) is given by

$$f(\mathbf{s}, t) = \sum_j C_j(t) f_j(\mathbf{s}) = \sum_j C_j(t)\langle\phi_j(\mathbf{r}; \mathbf{R})|e^{i\mathbf{s}\cdot\mathbf{r}}|\phi_j(\mathbf{r}; \mathbf{R})\rangle \tag{2.7}$$

Equation 2.7 implies that, for a sample composed of more than one electronic state, the instantaneous scattering amplitude is given by a sum of electronic-state scattering amplitudes, $f_j(\mathbf{s})$, each of which is weighted by its appropriate coefficient, $C_j(t)$.

The instantaneous X-ray scattering amplitude, $f(\mathbf{s}, t)$, directly reflects the electronic dynamics and indirectly reflects the nuclear dynamics since the electrons closely follow the nuclear motions. The evaluation of the exact scattering amplitude (eq 2.7) is at an unnecessary level of detail if our focus is only on the nuclear dynamics. Thus, in a manner similar to the single-electronic-state problem, we invoke the IAM and approximate the exact amplitude by a sum of atomic scattering amplitudes:

$$f(\mathbf{s}, t) = \sum_j C_j(t) f_j(\mathbf{s}) \approx \sum_j C_j(t)\sum_{\alpha=1}^{N} \exp(i\mathbf{s}\cdot\mathbf{R}_\alpha) f_j^\alpha \tag{2.8}$$

where f_j^α is the atomic scattering amplitude of atom α in electronic state j:

$$f_j^\alpha \equiv f_j^\alpha(\mathbf{s}) = \int d\mathbf{r}_\alpha \varphi_j^{\alpha *} \exp(i\mathbf{s}\cdot\mathbf{r}_\alpha)\varphi_j^\alpha \tag{2.9}$$

In eq 2.9, $\varphi_j^\alpha \equiv \varphi_j^\alpha(\mathbf{r}_\alpha; \mathbf{R}_\alpha)$ is the IAM electronic wave function of atom α in electronic state j, and for each electronic state j we have approximated the exact electronic wave function $\phi_j(\mathbf{r}; \mathbf{R})$ by a sum of such localized atomic electronic wave functions. At the end of this subsection, the implications of this assumption for the interpretation of time-dependent diffraction patterns are discussed. As implied by the IAM, there are no cross terms that involve electronic wave functions that are localized on different atoms and hence the innermost summation in eq 2.8 is just over all N atoms of the molecule. The equivalent equation for the electron scattering amplitude is easily derived by replacing the atomic X-ray scattering amplitude (eq 2.9) by the electron scattering amplitude:

$$g_j^\alpha \equiv g_j^\alpha(\mathbf{s}) = \frac{1}{s^2}[Z_\alpha - f_j^\alpha(\mathbf{s})] \tag{2.10}$$

The instantaneous X-ray scattering intensity (prior to integration over the nuclear coordinates) is given by the absolute value squared of its amplitude (eq 2.8):

$$\tilde{I}^{\text{inst}}(\mathbf{s}, t) = |\sum_j C_j(t) f_j(\mathbf{s})|^2 = \sum_{i,j} C_i^*(t) C_j(t)\sum_{\alpha,\beta} f_i^{\alpha *} f_j^\beta \exp[i\mathbf{s}\cdot(\mathbf{R}_\beta - \mathbf{R}_\alpha)] \tag{2.11}$$

and we have used the $\sim$ sign to indicate that the instantaneous intensity has not yet been integrated over the nuclear coordinates. In eq 2.11, the outermost double summation is over all electronic states in the sample whereas the innermost one is the usual double summation over all atoms in the molecule. As for the scattering amplitude, the equivalent expression for the electron scattering intensity is derived by replacing the atomic X-ray scattering amplitudes (eq 2.9) by the electron scattering amplitude (eq 2.10).

To evaluate the total scattering intensity, we need to average the instantaneous scattering intensity, eq 2.11, over the nuclear degrees of freedom and then integrate it over the time envelope of the incident X-ray or electron pulse. Equation 2.11 describes an $M \times M$ matrix (M is the number of electronic states in the sample) whose elements are given by $\tilde{I}^{\text{inst}}(\mathbf{s}, t)_{i,j} = C_i^*(t)C_j(t)f_i^*(\mathbf{s})f_j(\mathbf{s})$. The required averaging over the nuclear degrees of freedom therefore implies a right and left multiplication by the M dimensional vector of the nuclear wave function, $\chi(\mathbf{R}, t)$ [the jth element of this vector is the time-dependent nuclear wave packet of the jth electronic state, $\vec{\chi}_j(\mathbf{R}, t)$, cf. eq 2.6]:

$$I^{\text{inst}}(\mathbf{s}, t) = \sum_{i,j}\langle\chi_i(\mathbf{R}, t)|\tilde{I}^{\text{inst}}(\mathbf{s}, t)_{i,j}|\chi_j(\mathbf{R}, t)\rangle = \sum_{i,j} C_i^*(t)C_j(t)\langle\chi_i(\mathbf{R}, t)|f_i^*(\mathbf{s})f_j(\mathbf{s})|\chi_j(\mathbf{R}, t)\rangle = \sum_{i,j} C_i^*(t)C_j(t)\sum_{\mu,\nu} d_i^{\mu *}(t)\, d_j^{\nu}(t)\langle\chi_i^{\mu}(\mathbf{R})|f_i^*(\mathbf{s})f_j(\mathbf{s})|\chi_j^{\nu}(\mathbf{R})\rangle \quad (2.12)$$

[The reader can easily verify that for a one-electronic-state (and ro-vibrational nuclear state) wave function, eq 2.12 reduces to the IAM equation 2.1.] Finally, the scattering intensity for a noninstantaneous measurement, i.e., the X-ray or electron scattering intensity time integrated over the total diffraction pulse, is given by a weighted sum of the instantaneous scattering intensity (eq 2.12 and its electron equivalent) with the weights given by the time envelope of the incident X-ray or electron field intensity, $A(t, \tau)$

$$I(\mathbf{s}, \tau) = \int_{-\infty}^{+\infty} dt A(t, \tau) I^{\text{inst}}(\mathbf{s}, t) \quad (2.13)$$

As illustrated in Figure 1, the time envelope of the ultrafast X-ray or electron probe pulse, $A(t, \tau)$, is centered at time $t = \tau$, where τ is the time delay between the optical pump pulse and the diffraction probe pulse.

Equations 2.12 and 2.13 are the central equations of this paper, and we discuss them in some detail. We first consider the interference among ro-vibronic states. These can be divided into two classes: ro-vibronic interferences involving *different* electronic states and ro-vibrational interferences within a *single* electronic state. All these interference terms appear explicitly in the expressions for the instantaneous and total X-ray scattering intensity (eqs 2.12 and 2.13, respectively) and its electron equivalent. Due to the nature of the optical excitation (an ultrashort coherent laser pulse), the off-diagonal elements of the electronic, $C_i^*(t)C_j(t) = |C_i||C_j| \exp[i(\omega_j - \omega_i)t]$, ,and nuclear, $d_i^{\mu *}(t)\, d_j^{\nu}(t) = |d_i^{\mu}||d_j^{\nu}| \exp[i(\omega_j^{\nu} - \omega_i^{\mu})t]$, density matrices are nonzero and thus in principle the total scattering intensity (eq 2.13) does include products of scattering amplitudes that involve two different electronic and nuclear states. It implies that, in principle, the scattering *intensity* for a system composed of more than one electronic state is not given by the incoherent sum of the individual scattering intensities (weighted by the fractional populations of the states) but rather by a coherent sum that includes cross terms that are products of scattering amplitudes from different electronic states. In practice, one can observe such interferences only if the time resolution of the experiment, which is expected to be limited by the duration of the probe pulse, $A(t, \tau)$, is approximately of the order of or shorter than the oscillation period of these terms. This oscillation period, $\tau_{ij} = 2\pi/|\omega_j - \omega_i|$ is determined by the energy difference between the two states (i and j) in question and is thus very short for well-separated electronic states and much longer for vibrations and/or rotations. As a subpicosecond X-ray or electron pulse is still long when compared to the period $2\pi/|\omega_j - \omega_i|$ associated with the energy difference between two well-separated electronic states, we can assume that upon time integration over the envelope of the field intensity the cross electronic terms average to practically zero so that eq 2.13 reduces to

$$I(\mathbf{s}, \tau) \approx \sum_j I_j(\mathbf{s}, \tau) \quad (2.14)$$

where

$$I_j(\mathbf{s}, \tau) = \int_{-\infty}^{+\infty} dt A(t, \tau) n_j(t)\langle\chi_j(\mathbf{R}, t)|f_j^*(\mathbf{s})f_j(\mathbf{s})|\chi_j(\mathbf{R}, t)\rangle = \int_{-\infty}^{+\infty} dt A(t, \tau) n_j(t)\sum_{\mu} d_j^{\mu *}(t)\sum_{\nu} d_j^{\nu}(t)\langle\chi_j^{\mu}(\mathbf{R})|f_j^*(\mathbf{s})f_j(\mathbf{s})|\chi_j^{\nu}(\mathbf{R})\rangle \quad (2.15)$$

The equivalent expression for electron scattering is derived by replacing the X-ray scattering amplitude, $f_j(\mathbf{s})$, (in eq 2.15) with the electron amplitude:

$$g_j(\mathbf{s}) = \sum_{\alpha=1}^{N} g_j^{\alpha} = \sum_{\alpha=1}^{N} \frac{1}{s^2}(Z_{\alpha} - f_j^{\alpha}(\mathbf{s})) \quad (2.16)$$

The approximation (2.14) to the scattering intensity is the result that has been assumed (and never really derived) in all previous studies of ultrafast gas-phase electron diffraction. Since its derivation is quite long (eqs 2.9−2.14), it is useful to reiterate the two basic steps that led to it: (i) the instantaneous X-ray and electron scattering intensities were computed for a coherent multi-electronic-state system (eqs 2.6−2.12). (ii) These instantaneous intensities were integrated over the total diffraction pulse with the weights given by the time envelope of the incident probe (X-ray or electron) field (eqs 2.13−2.16). Although we too will use eq 2.14 in our numerical examples, we note that this is an approximation that will break down when electronic surfaces approach one another, for example, in curve crossing, and more generally whenever the duration of the probe X-ray or electron pulse is comparable to the period associated with the energy difference between two electronic states.

Finally, we consider the implications of using the IAM in time-dependent diffraction studies. The dynamics of atoms and molecules, particularly in chemical reactions, involve the dynamics of both the nuclei and of the electrons. As seen from eq 2.6, in principle, both are reflected in ultrafast X-ray and electron diffraction. If we consider, for example, the cleavage of a diatomic bond, then the electronic density deforms from a peanutlike shape (where the valence electrons are partially localized between the two atoms) to two clouds that are localized about the two separated atoms. The IAM does not allow for such deformations of electronic densities, and hence, the time dependence is associated only with the nuclear motion: the localized electronic cloud is assumed to remain spherical and nonoverlapping, instantaneously adjusting itself to the changing nuclear positions. Thus, the IAM time dependence of the X-ray diffraction pattern does not reflect bonding changes in valence electrons. Although in the future it may be possible to experimentally measure such electron dynamics, it will be a more difficult task than measuring the nuclear dynamics where the required spatial resolution is lower and where the information is carried by the scattering from all the electrons instead of just by the valence electron scattering. The diffraction pattern is dominated by the nearly spherical core electronic clouds, and under usual circumstances one cannot separately discern the few bonding electrons. Thus, the IAM approximation is usually reasonable. There are, however, clear cases where the basic

IAM picture breaks down and a more detailed approach is needed, for example to treat the time-dependent migration of charge during a charge-transfer reaction.

B. Time-Dependent Diffraction from a Two-Electronic-State Diatomic Molecule. As a more specific simple illustration of the general formulas derived in the previous subsection, we discuss diffraction for the special case of an ultrafast electronic excitation of a homonuclear diatomic molecule in the gas phase. While we explicitly write out only the X-ray case, the electron diffraction case can be easily written out in a parallel manner. Two electronic states (the indices 1 and 2 refer to the ground and excited states, respectively) are included in the electronic expansion, and by transforming the two-atom homonuclear system to a relative coordinate system,[81] $\mathbf{R} = \mathbf{R}_\alpha - \mathbf{R}_\beta$, the instantaneous scattering intensity is written as a sum of four terms:

$$I^{\text{inst}}(\mathbf{s}, t) = 2\sum_{i,j=1}^{2} C_i^*(t)C_j(t)f_i^*(\mathbf{s})f_j(\mathbf{s})\langle\chi_i(\mathbf{R}, t)|1 + \cos(\mathbf{s}\cdot\mathbf{R})|\chi_j(\mathbf{R}, t)\rangle \quad (2.17)$$

and the intensity integrated over the diffraction pulse as a sum of two terms:

$$I(s, \tau) = 2\int_{-\infty}^{+\infty} dtA(t, \tau)n_1(t)|f_1(\mathbf{s})|^2\langle\chi_1(\mathbf{R}, t)|1 + \cos(\mathbf{s}\cdot\mathbf{R})|\chi_1(\mathbf{R}, t)\rangle$$

$$+ 2\int_{-\infty}^{+\infty} dtA(t, \tau)n_2(t)|f_2(\mathbf{s})|^2\langle\chi_2(\mathbf{R}, t)|1 + \cos(\mathbf{s}\cdot\mathbf{R})|\chi_2(\mathbf{R}, t)\rangle \quad (2.18)$$

In writing eq 2.18, we have assumed that cross products of scattering amplitudes from different electronic states average to zero (cf. eqs 2.14 and 2.15). (Note also that here and in what follows, **R** is a three-dimensional vector that denotes the internuclear separation vector between the two atoms.) The fractional populations, n_j, of the different electronic states are determined by the optical excitation. Prior to the application of the optical pump pulse, only the ground state ($j = 1$) is populated and causes scattering. Once we excite part of the ground-state population to the excited electronic state, the scattering intensity is given by a weighted sum of ground- and excited-state scattering intensities, with the weights given by the fractional populations.

The scattering intensities that we compute in section III are evaluated using eq 2.18. We reiterate that electronic cross-scattering amplitudes exist in principle at the scattering intensity level, eq 2.12, but can be assumed to average to zero when the two electronic states are well separated in energy (see discussion following eq 2.13).

The evaluation of the scattering intensity requires as an input the three-dimensional time-dependent nuclear wave function, cf. eq 2.18. We choose an initially isotropic gas-phase sample as a simple illustration. Prior to the optical excitation we assume that the ground state is spherically symmetric (i.e., all the different M states of a given rotational level are equally populated). Once we apply the optical pulse, this spherical symmetry is broken as the optical pump pulse creates a "hole" in the initial isotropic distribution. Furthermore, the ultrafast excitation also creates a coherent superposition of rotational levels in the excited-state vibrational manifold. (The amplitudes of the vibrational states are determined by the detailed shape of the pump pulse; see section III.A below.) For ease of computation, we approximate the nuclear wave function, $\chi_j(\mathbf{R}, t)$, as a product of an angle-independent radial part, $\chi_j(R, t)$, and an angular part, $Y_j(\theta, \varphi, t)$. [The polar angle θ is the angle between the internuclear vector **R** and the lab frame Z axis, and the azimuthal angle φ is the projection (with respect to the Z axis) of the internuclear vector on the lab XY plane.] In the Appendix we provide analytical expressions for the rotational part of the wave functions for both the ground and the excited states, assuming a single-photon process for the latter (i.e., first-order perturbation theory) and a two-photon process for the former (i.e., second-order perturbation theory). It should be noted that the two assumptions that we make (radial part is independent of the angular part and computing the latter using first- and second-order perturbation theory) are approximations and in particular cycling between the ground and excited states can result in angular distributions that are tighter than predicted by first- and second-order perturbation theory.[83] Since the sample is of diatomic molecules, we limit our discussion to two cases: a parallel transition, $\Delta J = \pm 1$, $\Delta\Lambda$ and $\Delta M = 0$, (electronic transition dipole parallel to the internuclear axis) and a perpendicular transition, $\Delta J = 0, \pm 1$, $\Delta\Lambda = \pm 1$, and $\Delta M = 0$ (dipole perpendicular to the internuclear axis.[84]) [J is the total angular momentum, Λ the molecule fixed (in the diatomic case electronic) component along the internuclear axis, and M the component in the chosen space fixed direction.] Here we only outline the various steps and discuss the final result.

First we write the three-dimensional nuclear wave function as a product of a radial part and an angular part. The discussion of the radial part is deferred to section III.A and here we only note that the one-dimensional quantum computation gives both the time-dependent radial part of the two electronic-state wave function and the time-dependent ground- [$n_1(t)$] and excited- [$n_2(t) = 1 - n_1(t)$] state fractional populations. The angular part of the wave function (of both the ground and the excited state) is written as a coherent sum over rotational eigenstates whose amplitudes are computed using the Clebsch−Gordan series and its inverse.[85,86] (Note that whereas the excited-state rotational wave packet is fully coherent, the ground-state rotational wave packet is only partially coherent because the optical excitation creates a hole in the initially isotropic distribution.) Next, the three-dimensional Fourier transform, eq 2.18, is reduced to a one-dimensional numerical integration by expanding the $\cos(\mathbf{s}\cdot\mathbf{R})$ in terms of products of even spherical harmonics and spherical Bessel functions (cf. eqs A.13 and A.16). Using the orthonormality of the rotational wave functions and the Clebsch−Gordan series, the integrals over three spherical harmonics [two from the rotational eigenfunctions and one from the expansion of $\cos(\mathbf{s}\cdot\mathbf{R})$] are evaluated analytically and written in terms of products of Clebsch−Gordan coefficients.[85,87] This procedure is applied for both the ground and excited states. In analogy to optical pump−probe experiments, this results in a scattering intensity that is a sum over even products of spherical Bessel functions [$j_l(sR)$] with Legendre polynomials, $P_l(\hat{\mathbf{s}}\cdot\hat{\mathbf{e}})$, in the angle, γ, between the optical polarization unit vector, $\hat{\mathbf{e}}$, and the scattering vector **s**, $\cos\gamma = \hat{\mathbf{s}}\cdot\hat{\mathbf{e}}$. ($\hat{\mathbf{s}}$ is the unit scattering vector whose two lab frame polar coordinate angles determine the scattering direction, see Figure 2):

$$I_j(\mathbf{s}, \tau) = 2\int_{-\infty}^{+\infty} dtA(t, \tau)n_j(t)|f_j(s)|^2\left[1 + \sum_{l=0}^{\infty}(i)^l 4\pi\sqrt{\left(\frac{2l+1}{4\pi}\right)}P_l(\hat{\mathbf{s}}\cdot\hat{\mathbf{e}})\,\Xi_l(t)\,\langle\chi_j(R, t)|j_l(sR)|\chi_j(R, t)\rangle\right] \quad (2.19)$$

where

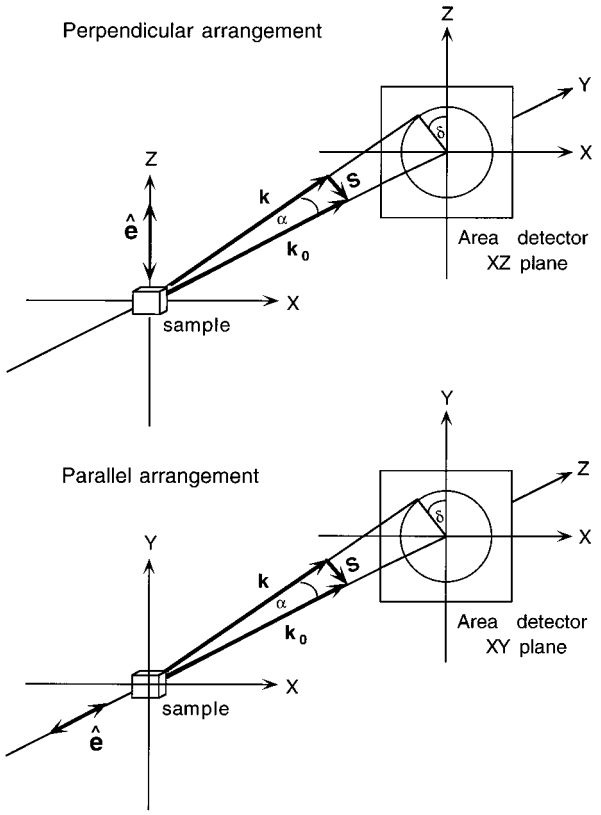

Figure 2. Upper drawing: Schematic of the perpendicular experimental arrangement simulated in the computations. The polarization vector ($\hat{\mathbf{e}}$) of the optical pulse (Z axis) and the propagation direction of the incident ($\mathbf{k}_o$) X-ray or electron beam (Y axis) are perpendicular. X-ray photons or electrons with the wave vector $\mathbf{k}$ scatter at angle α and intersect the (XZ) plane of the detector at angle δ. The scattering vector $\mathbf{s}$ is the difference between the incident and scattered wave vectors. In the parallel arrangement (lower panel) the optical polarization vector is parallel to the incident X-ray or electron propagation vector (along the Z axis) and the area detector is placed in the XY plane.

$$\Xi_l(t) = \langle Y_j(\theta, \varphi, t) | Y_{l0}(\theta, \varphi) | Y_j(\theta, \varphi, t) \rangle \qquad (2.20)$$

In eq 2.20, $Y_j(\theta, \varphi, t)$ is the time-dependent angular wave function of the jth electronic state (cf. eq A.3) and $Y_{l0}(\theta, \varphi)$ is a $J = l$, $M = 0$ spherical harmonic function. Because of the even symmetry in our problem (a homonuclear diatomic molecule has an inversion symmetry which the dipole interaction with the electric field does not alter), only even l states contribute to the sum in eq 2.19 whose upper bound, $(2J + 2)$, is determined by the Clebsch−Gordan theorem. In practice we find that this sum converges quite rapidly. Physically, the "classical-like" behavior of the rotational motion is the reason for this fast convergence. (In the classical limit only $l = 0$ and 2 states contribute to the sum in eq 2.20.) As noted in the Appendix, and illustrated in Figure 2, the angle γ depends on the details of the experimental arrangement, and just as in any optical pump−probe experiment, two different experimental arrangements, parallel (lower drawing in Figure 2) and perpendicular (upper drawing in Figure 2), should be considered.[57,70] In the parallel configuration, the optical polarization vector $\hat{\mathbf{e}}$ is parallel to the incident X-ray or electron propagation wave vector $\mathbf{k}_0$, and hence the laser and X-ray or electron beams must be perpendicular in their propagation direction. In the perpendicular arrangement the two beams may co-propagate so that the optical polarization vector is perpendicular to $\mathbf{k}_0$. These two arrangements give significantly different results (cf. eqs A.12 and A.15) because the system is now symmetric only about one axis that of the optical polarization.[16,70] Hence, when the propagation axis and the optical axis do not coincide, i.e., a perpendicular arrangement, the scattering pattern loses its cylindrical symmetry because the spatial distribution (of both the ground and the excited states) is symmetric with respect to the polarization vector $\hat{\mathbf{e}}$ but it is not symmetric with respect to rotation about the axis of the incident probe beam, $\mathbf{k}_0$. Experimentally, in particular for the X-ray case, the perpendicular arrangement is more amenable to short-time resolution, because the optical and X-ray pulses can co-propagate in synchrony in the sample. It also offers more information, as the noncircular shape of the diffraction pattern will be used in section IV to separate the diffraction signal of the excited state from that of the ground state. Hence, in the next section we only discuss the perpendicular arrangement.

If one considers a thermal ensemble of ground-state molecules to which our excitation pulse is applied, then any initial ground ro-vibrational eigenstate results in a particular coherent superposition on the excited state. As argued above, the latter is determined by the nature of the excitation pump pulse and by the rotational selection rules. This implies that the diffraction intensity should be computed, using eq 2.18, for each of these initial states (and the resulting excited states). The total, thermally averaged, diffraction intensity is then given by the Boltzmann average of these diffraction intensities.[47] (Note that this average is performed on the level of intensities and not amplitudes since the ground state is assumed to be thermal, i.e., in terms of its nuclear ro-vibrational density matrix the off-diagonal elements average to zero.) The small spacing between rotational levels combined with their $(2J + 1)$ degeneracy results at room temperature in a rotational distribution that peaks for bromine, for example, at $J = 35$.

III. Numerical Examples

Two simple examples of bound and dissociative motion in a diatomic molecule are discussed in this section, using respectively, I_2 (where ultrafast diffraction has previously been considered from a classical viewpoint by our group[15,16] and by Williamson and Zewail[70]) and Br_2. Special reference is given to the breaking of symmetry in the system by the linearly polarized optical pump pulse. This symmetry breaking is further used in the next section where we show how to isolate the excited-state dynamics from that of the ground state using the symmetry of the electronic transition.

A. Technical Details. Our computation attempts to provide a realistic quantum modeling of an optical pump−diffraction probe experiment. We begin the simulation with all the population on the ground electronic surface. This state is then coupled to an excited electronic state via an external optical field: a temporally Gaussian-shaped pulse with fwhm of 70 fs, intensity of 2×10^{11} W/cm^2, and a wavelength of 400 nm (25 000 cm^{-1}) for Br_2 and 520 nm (19 320 cm^{-1}) for I_2. The radial part of the time-dependent Schrödinger equation is solved numerically (for this two-electronic-state system) using the Newton interpolating polynomial and Fourier techniques.[88] This computation provides the time-dependent vibrational part of the nuclear wave function, $\chi_j(R, t)$, as well as the electronic-state fractional populations, $n_j(t)$. [Note that, strictly speaking, the exact population depletion is given by the product of $n_j(t)$ and a geometric factor which we compute in the Appendix.] The angular part (which is also time-dependent) is evaluated analytically using the appropriate selection rules (see previous section and the Appendix). At each point in time, we then write the nuclear wave function (for each electronic state) as a product of a radial part and an angular part. The two-electronic-state time-dependent diffraction pattern is computed using eqs 2.18−

2.20 for various (increasing) pump−probe delay times, τ. Probe X-ray pulses with fwhm between 100 and 300 fs are used and a wavelength of either 154 or 56.1 pm (corresponding to the Cu and Ag Kα lines, respectively). As discussed in the previous section, only the perpendicular pump−probe arrangement is considered and thus, as shown in the upper panel of Figure 2, the optical laser pulse is polarized along the lab frame Z direction, the incident X-ray beam propagates along the Y direction, and an area detector is placed in the XZ plane. In the present computation, we use the same atomic form factor for both the ground and the excited states, i.e., $f_1(\mathbf{s}) = f_2(\mathbf{s})$ (this is a reasonable approximation for the heavy atoms discussed in this paper), and the diffraction intensities are averaged over the ground-state rotational distribution. For simplicity, we treat only a single vibrational state in the initial ground electronic-state distribution. Extension to an average over an initial vibrational distribution is straightforward.

Before we discuss the results, we consider the role of rotation. As discussed in detail in the previous section and elsewhere,[15,16,57,70] the pump laser pulse converts the isotropic sample into an anisotropic mixture of two electronic states. Immediately after a perpendicular (parallel) transition, the excited-state internuclear axes are aligned predominantly perpendicular (parallel) to the polarization vector of the optical field, whereas the ground state is depleted in this direction. The exact amount that is depleted (excited) is determined by the excitation probability multiplied by a geometric factor ($^1/_3$ for a parallel transition and $^2/_3$ for a perpendicular one). At any time t after the excitation, the angular distribution (of both the ground and the excited states) is determined by the time evolution of the coherent superposition of rotational levels in the ground and excited electronic-state vibrational manifolds. As both states are composed of different rotational levels that have different rotational periods, this initial rotational coherence decays on the picosecond time scale.[70] (Under collisionless conditions one can observe the relocalization of rotational coherences and this relocalization does not vanish upon thermal averaging.[89]) This delocalization of the rotational coherences is expected to progressively reduce the observed changes in the anisotropy of the diffraction pattern. In the present computation, we average over 50 ground-state rotational levels (and all the corresponding M levels) and still observe significant changes in the diffraction pattern and in particular the effect of anisotropy. This somewhat weak sensitivity to rotational motion is due to a combination of two effects. First, the heavy masses of the atoms implies a slow rotational period and hence we do not expect to see a significant reduction in the anisotropy at short times. This is even more so in the case of dissociative motion where the excited-state explodes apart very rapidly, freezing in the angular distribution. (A classical computation shows that for excitation at 400 nm an excited-state bromine molecule formed at $J = 35$ rotates by only 4° from its initial configuration as the atoms separate. In our computation for the bromine molecule, we therefore assume that the excited state is frozen at its initial angular distribution determined by the rotational selection rules. For the iodine molecule, we make no such assumption and both the ground and excited states are allowed to rotate.) The second effect is due to the ground state (which in the example of dissociative motion is in practice the only one that is appreciably rotating). As the effect of the ground-state anisotropy is only second order in the field (see the discussion in the previous section and the Appendix), it is of somewhat less importance. We do note, however, that since the radial part of the wave function is assumed to be angular momentum independent (i.e., we ignore vibrational−rotational coupling, for example the J-dependent centrifugal term in the internuclear potential) our computation underestimates the role of rotational delocalization.

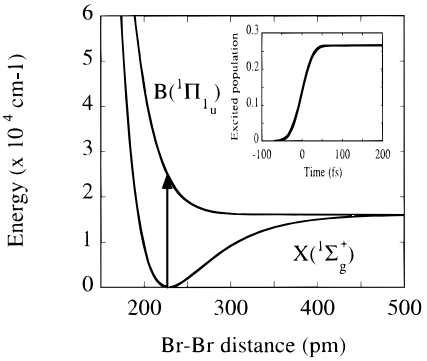

Figure 3. The ground, $X(^1\Sigma_g^+)$, and excited, $B(_1\Pi_{1_u})$, electronic state potentials of the bromine molecule (as a function of internuclear distance) used in the computations. The arrow illustrates the electronic excitation (25 000 cm^{-1}), and the inset shows the excited-state fractional population as a function of time in fs, for a transform-limited Gaussian-shaped pulse of 70 fs fwhm duration. The steep excited-state potential curve results in very rapid dissociation.

B. Results. 1. Br_2. To be able to observe the detailed atomic motions by which chemical reactions take place, one needs a probe X-ray or electron pulse whose time duration is similar and preferably shorter than that of the making and breaking of chemical bonds. (An alternative would be to use time-resolved detection.) Ideally one would therefore like to be able to produce and measure ≤100 fs X-ray and electron pulses. Since streak cameras for measuring X-ray or electron pulse duration do not have this time resolution, the main objective of the first example that we discuss is to provide a nonconventional (yet hopefully feasible) procedure for measuring the time profile of ultrafast probe X-ray or electron pulses. We suggest the use of a fast chemical reaction as a clock.[37−39,48] Our example "chemical clock" is the simplest chemical reaction, the photodissociation of a homonuclear diatomic molecule: $Br_2 \rightarrow Br + Br$. In Figure 3 the potential energy curves[84,90] for the two electronic states (along with an arrow that indicates the electronic transition) are shown. An ultrafast optical pulse pumps the ground $X(^1\Sigma_g^+)$-state molecule into a steeply dissociative $^1\Pi_{1_u}$ state. As a result, the dissociation of the diatomic molecule is very rapid. For our specific choice of pulse duration and intensity (70 fs fwhm and 2×10^{11} W/cm^2), about 26% of the ground-state population is pumped into the excited state, as shown in the inset to Figure 3. To characterize the X-ray (or similarly electron) pulse, we first compute the diffraction pattern (for Cu Kα 154 pm X-rays) as a function of time at a specific angle (α, δ; see Figure 2) where the change in intensity is predicted to be most pronounced. Hence, in the case of bromine, where the electronic transition is perpendicular, we choose the azimuthal angle δ to be in the direction perpendicular to the optical polarization. The polar angle α is set to the first crest in the ground-state molecular diffraction. In an ideal hypothetical experiment one would like to be able to record the diffraction intensity [at a given (α, δ)] of only the ground, or excited, state. As a function of time one would then observe a simple steplike depletion, or rise, in the scattering intensity as the latter would be proportional to the scattering population (see eq 2.15, for example). In general, however, both states will contribute to the time-dependent diffraction intensity. Thus, to still be able to use the photodissociation reaction as a "chemical clock", the diffraction intensity with contributions from both states should still exhibit pronounced changes in intensity (as a function of time) that can be detected in an experiment with a reasonable

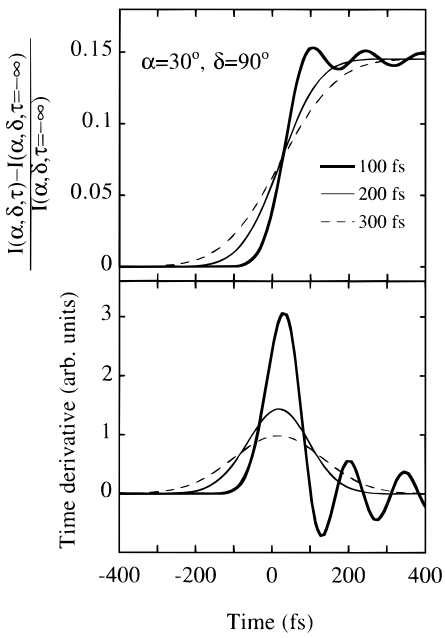

Figure 4. Upper panel: the variation in diffraction intensity as a function of delay time τ (in fs) for molecular bromine at an angle of $\alpha = 30°$ and $\delta = 90°$ using three Gaussian-shaped X-ray probe pulses of different fwhm time duration: 100 (full thick line), 200 (full thin line), and 300 (dashed line). (In all three cases, the duration (fwhm) of the optical pump pulse is 70 fs.) The polar angle, α, corresponds to the first crest in the ground-state molecular diffraction, and the azimuthal angle, δ, is chosen perpendicular to the polarization direction of the optical light. In this figure (and in all the other scattering figures and differences thereof), both the ground and the excited states contribute to the diffraction intensity (see eq 2.18) and the changes in intensity (or differences thereof) as a function of time are predominantly due to the excited-state dynamics. Because the photodissociation dynamics is very rapid, the time profile of the change is governed by the duration of the probe X-ray pulse, thereby suggesting that a fast chemical reaction can be used as a tool to measure the duration of the probe X-ray or electron pulse. Lower panel: the time derivative of the variation in diffraction intensity shown in the upper panel, which measures the X-ray pulse envelope. The oscillations shown for the 100 fs pulse could be eliminated by a more sophisticated treatment.

signal-to-noise ratio. An easily readable "chemical clock" requires that the time profile of the diffraction intensity be governed by the duration of the probe pulse (in other words, we would like the X-ray or electron pulse duration to be long with respect to the optical pump duration and the time scale of the observed molecular dynamics). In the upper panel of Figure 4, we compute the difference in diffraction intensity as a function of time using three X-ray probe pulses with varying time duration (100, 200, and 300 fs). [In this figure and all the other diffraction intensity (and differences thereof) figures, the intensity is computed using eq 2.18 and the changes in intensity as a function of time are predominantly due to the excited-state dynamics.] This figure confirms our suggestion that a simple chemical reaction can be used as a tool to measure the duration of the probe X-ray pulse: although both states scatter, the intensity does change rapidly as a function of time and the time profile of the change is governed by the probe pulse and not by the photodissociation dynamics. To better illustrate this point we also show the time derivative of the change in intensity, lower panel of Figure 4, which approximately, but quite well, measures the X-ray pulse envelope. As shown in eq 2.16, this time profile convolutes in it both the time dependence of the probe X-ray pulse, $A(t, \tau)$, and the time dependence of the nuclear dynamics, $I_{\text{inst}}(\mathbf{s}, t)$. If the latter is known theoretically, one can deconvolute this time profile to recover more accurately the time profile of the probe X-ray pulse. The distinct oscillations in intensity (upper panel of Figure 4), observed only with the shorter probe pulse, are due to the dissociative dynamics on the excited electronic state. Again they could be removed from the lower panel curve by a more accurate deconvolution procedure. Their qualitative features can be reproduced by invoking an Ehrenfest type of approximation for the scattering intensity, i.e., by replacing the expectation value of the scattering intensity by the scattering intensity at the average position of the wave packet.

In this initial example, a fast chemical reaction has been chosen so that the time resolution is predominantly determined by the probe X-ray pulse. Once the probe X-ray pulse is characterized, one would prefer to shift the emphasis to measuring molecular dynamics rather than pulse duration. Thus, it is worthwhile to compute the diffraction intensity as a function of time and see if we can discern observable changes that can be detected using X-ray pulses with nonzero duration. Hence, in Figure 5 we show a series of Cu Kα diffraction patterns at various pump−probe delay times. (Note that because we are probing a dissociative motion (leading to large spacing between the two bromine atoms) we observe changes as a function of time at small diffraction angles. At larger scattering angles, $\alpha > 20°$, the changes occur at very early times after which the intensity is basically constant; cf. Figure 4.

In the uppermost panel of Figure 5, we show the computed initial diffraction pattern of ground-state molecular bromine. (This is the total scattering intensity and not only the "molecular" part.) For the initially isotropically distributed molecules, the pattern is cylindrically symmetric. As argued above and shown in Figure 4, once the molecule interacts with the optical pump field, one expects to see changes in this pattern. The other panels in Figure 5 show a series of diffraction patterns at increasing pump−probe time delays. Even though these patterns have been evaluated using a Cu Kα (154 nm) 200 fs X-ray probe pulse, and thermally averaged over the ground-state rotational distribution, at certain small diffraction angles the changes in intensity are substantial. (Experimentally this result is encouraging since the intensity decreases very rapidly with the scattering angle and thus the signal is higher at small angles.) The magnitude of these changes is determined by three factors: (i) the amount of excited-state fractional population, (ii) the radial part of the nuclear wave function, and (iii) the angular part. The more population that is excited, the larger the changes. The effect of the radial wave function is twofold: the larger the difference between the ground- and excited-state internuclear distributions the more pronounced are the differences in the diffraction pattern. (A dissociative excited state therefore serves as a very favorable example.) The width of the radial wave function also affects the diffraction pattern: the more localized the wave function, the sharper the observed pattern. (In the present example the ultrafast excitation into the $^1\Pi_{1_u}$ state establishes a localized nonstationary vibrational state whose subsequent evolution can be well approximated at the short times treated here by an ensemble of classical trajectories.) The role of the angular part is discussed in detail in the Appendix.

2. I_2. To check the effects on the diffraction pattern of radial delocalization and of the similarity between ground- and excited-state radial wave functions, it is useful to look at a bound motion in a diatomic molecule where at certain points in time the ground- and excited-state internuclear distributions may be similar and in addition the latter may at different times show considerable delocalization (due to the nature of the optical excitation and the potential surfaces). Since molecular iodine

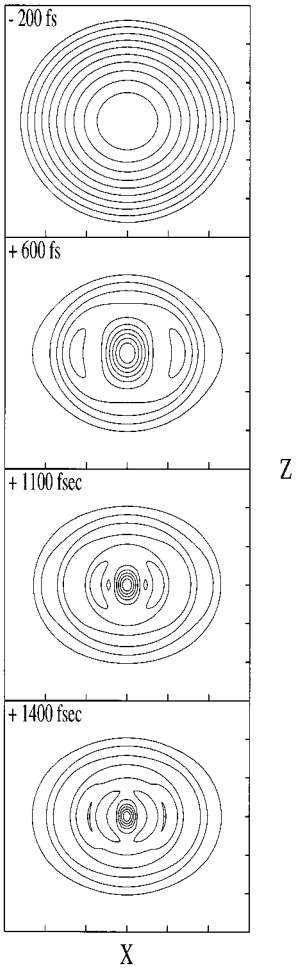

Figure 5. Two-dimensional polar contour plots (arbitrary units) of X-ray scattering intensities of molecular bromine at a series of increasing pump−probe time delays, τ, measured between the centers of the 70 fs optical pump and the 200 fs Cu Kα (154 pm) X-ray probe pulses. The pump and probe pulses co-propagate, i.e., a perpendicular pump−probe arrangement (see Figure 2). Here, and in all subsequent scattering (and differences thereof) figures the horizontal axis is *X* and the vertical is *Z*, as in Figure 2. The results are averaged over the ground-state rotational distribution, and the contours are equally spaced. The distance from the origin to any point on the graph is the scattering angle α (a circle inscribed within the bounding box would be at a scattering angle of 20°), and the angle between this line and the vertical *Z* axis is the azimuthal angle δ ($0 \le \delta \le 2\pi$). The changes in intensity as a function of time are mainly due to the time evolution of the excited state and because we are probing a dissociative motion (large internuclear distances) the changes are concentrated at small diffraction angles. The most pronounced features in these diffraction patterns are the collapse of the scattering intensity toward smaller diffraction angles and the anisotropy in the azimuthal angle induced by the interaction with the polarized pump pulse. Note that, because the molecular electronic transition dipole is perpendicular to the internuclear axis (a perpendicular transition), the changes in intensity are most pronounced in the direction perpendicular to the optical polarization direction.

has been the subject of numerous pump−probe experimental and theoretical studies,[15,16,70,91−95] and its relevant potential energy surfaces are well-known,[84,96] we use it as an example. An iodine molecule is excited from the ground *X* state into the bound region of the excited *B* (O_u^+) state and the system is probed via either X-ray (Figure 7) or electron (Figure 8) diffraction at two delay times, 215 and 435 fs after the optical excitation. (The duration of the probe X-ray and electron pulses is 100 fs.) Snapshots of the ground- and excited-state wave functions at these two delay times (as well as the relevant potential energy surfaces) are shown in Figure 6. At 215 fs

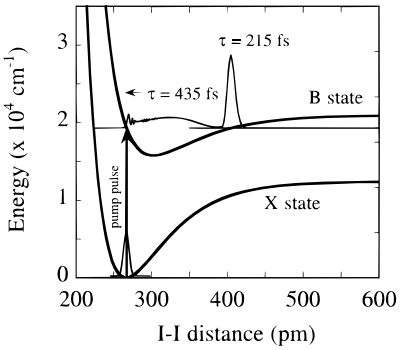

Figure 6. The ground, *X*, and excited, *B*, electronic-state potentials of I_2 as a function of internuclear distance (in pm). An ultrafast pump pulse with a carrier frequency of 19 230 cm^{-1} excites the ground, *X*, state molecule into the bound region of the excited *B* state. About 15% of the population (not shown) is excited. Superimposed on the potentials are the ground-state wave function (before the excitation) and two "snapshots" of the excited-state wave function (215 and 435 fs after the electronic excitation).

the ground- and excited-state wave functions are localized at very different internuclear distances, and indeed, if we look at a difference (τ = 215 fs minus $\tau = -\infty$) scattering intensity plot (upper panels in Figures 7 and 8), we see that the differences are significant (the highest and lowest difference contours are drawn at 0.04 and −0.04, respectively, compared to the highest X-ray diffraction intensity at forward scattering of 1.) On the other hand, at τ = 435 fs, when the ground and excited states are at more similar internuclear distances and in addition the excited state is delocalized (see Figure 6), the difference (τ = 435 fs minus $\tau = -\infty$) in the X-ray and electron scattering intensity is less pronounced (lower panels of Figures 7 and 8). Comparing Figures 7 and 8, note how similar the X-ray and electron difference results are, illustrating the fundamental theoretical similarity of X-ray and electron diffraction. For both, the changes in the diffraction intensity are greater along the direction of the optical polarization (the *Z* axis), as expected for a parallel transition. (We do note, however, that the two figures would be less similar had electronically inelastic scattering been included in the calculation, a point that needs to be treated more deeply for time-dependent diffraction than we have done here.)

The initial coherent vibrational motion (and subsequent delocalization) of ultrafast pumped iodine has been extensively studied using ultrafast optical spectroscopy.[92,94,95] In a typical ultrafast optical experiment, the excited-state dynamics are probed by monitoring the laser-induced fluorescence from a third electronic state into which the excited *B* state molecule is promoted by the probe pulse. Although the most common (and intuitive) observable that one would like to derive when discussing coherent vibrational motion is the expectation value of the position on the excited electronic state, none of these time domain experiments (and their frequency domain analogues) probe this observable directly. On the other hand, inverse **k** (momentum) space (the domain of diffraction experiments) and real **r** (coordinate) space are directly related by a Fourier transform. In Figure 9, we plot the difference in the X-ray diffraction intensity (at the fixed scattering angle for which, on the basis of Figure 7, we expect to see large changes) as a function of time (dashed line and right axis), as well as the expectation value of the position on the excited electronic state (full line and left axis), $\langle R(\tau) \rangle$, from the quantum dynamics. The coherent motion of the excited state and its subsequent delocalization is reflected in the single-angle time-dependent diffraction intensity in a manner almost identical with $\langle R(\tau) \rangle$.

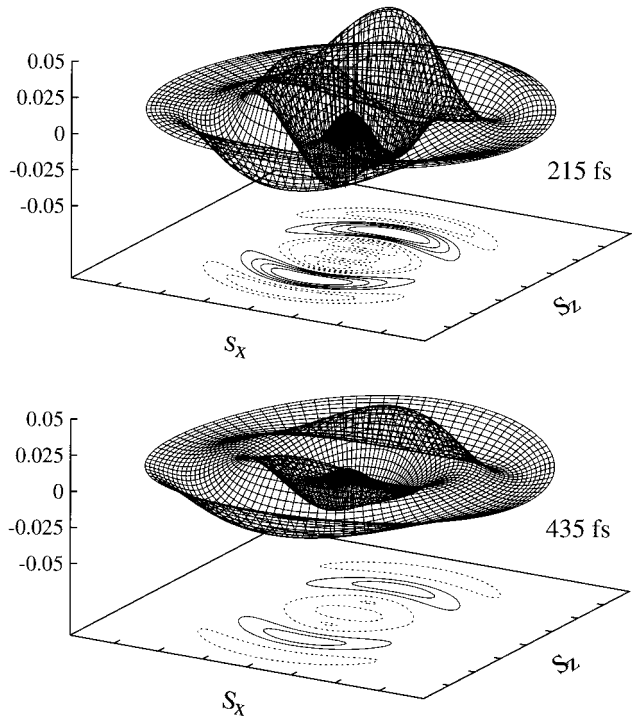

Figure 7. Three-dimensional polar contour plots for molecular iodine at two pump−probe delay times of the X-ray scattering intensity at that delay time minus the intensity for the unpumped ground state. (The excited-state wave functions at these two time points are shown in Figure 6, and the duration of the probe X-ray pulse is 100 fs, fwhm.) The solid (dashed) contours are equally spaced (0.01 apart) between 0.01 (−0.01) and 0.04 (−0.04) with the highest (absolute) value being the innermost one. The scattering vector **s** for a circle bounded by the box of the figure is 4.0 Å^{-1} for both panels. (The magnitude of the scattering intensity at forward scattering does not depend on time and for undifferentiated data equals 1.) As expected for a parallel transition, the intensities in these difference plots are greater along the optical polarization direction (*Z* axis). Their magnitude reflects the width of the ground- and excited-state wave functions and the extent of their overlap in space. When the ground and excited states are at different internuclear distances, and both are localized (upper panel), see Figure 6, the differences in intensity are most significant (the highest and lowest values in the upper panel are 0.04 and −0.04, respectively). When they are at similar distances, lower panel, and furthermore the excited-state wave function is delocalized (see Figure 6), the differences are less pronounced (the highest and lowest values in the lower panel are 0.02 and −0.02, respectively).

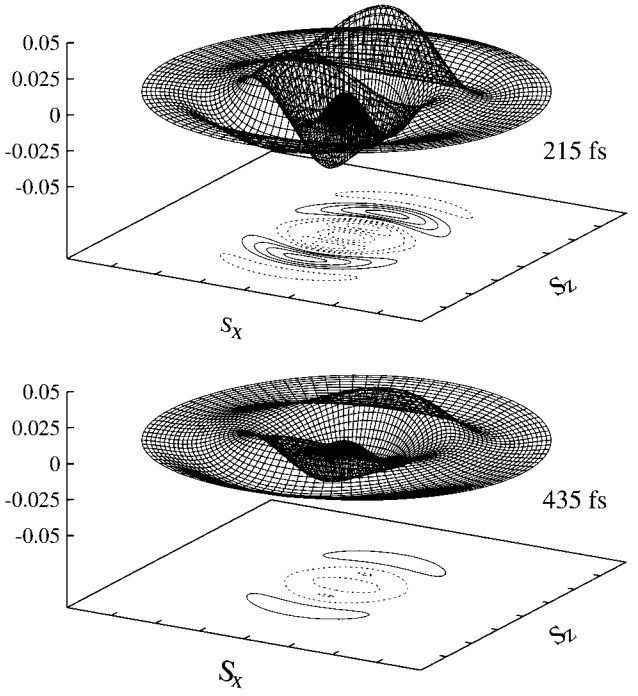

Figure 8. As in Figure 7 but for electron diffraction substituting the electron scattering amplitude, $g_j(\mathbf{s})$, [from eq 2.10], for the X-ray scattering amplitude, $f_j(\mathbf{s})$, in eq 2.18. The vertical and horizontal scales in these two plots are the same as in Figure 7, and the contours (both dashed and solid) are drawn at the same values as in Figure 7. Note that these difference plots for electron diffraction are very similar to those for X-ray diffraction, Figure 7, reflecting the similarity of their theoretical foundations.

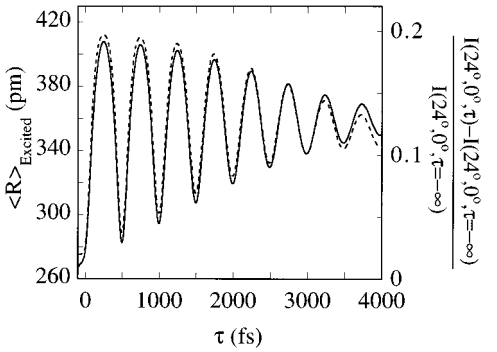

Figure 9. Normalized difference diffraction intensity at $\alpha = 24°$, $\delta = 0°$ (right axis and dashed line) compared to the quantum expectation value of the internuclear distance (left axis and solid line) on the excited electronic state as a function of delay time τ for molecular iodine. (In this figure, the difference in diffraction intensity is defined as the intensity at time τ minus the intensity before the optical excitation, the result being divided by this last value.) The probe X-ray pulse duration is 100 fs, fwhm. That the difference in diffraction intensity at just a single angle reflects so clearly the initial coherent vibrational motion and subsequent vibrational delocalization shows the direct and close relationship between time-resolved diffraction experiments and nuclear dynamics.

(Note again that the diffraction intensity used to produce this figure is computed for a sample that consists of *both* ground- and excited-state molecules, using eq 2.18.) This figure demonstrates that ultrafast diffraction experiments can be used as direct, real-time, probes of nuclear dynamics. In the next section we will continue this discussion by showing the inversion of the time-dependent data from **k** space to real space.

We now return to the role of rotation. In these two examples (and in particular in the bromine case), the excited state does not appreciably rotate and the ground state is rotating slowly compared to the time periods illustrated in Figures 3−9. (Care should be taken when discussing Figure 9 whose time scale is somewhat longer; see below.) Thus, the effect of the rotational dynamics is somewhat diminished. We reiterate that this is not a general result, and we do expect the rotation to play a more significant role in other reactions. Furthermore, we point out that our neglect of the coupling between vibration and rotation underestimates the role of rotation in delocalization and thus expect the loss of vibrational coherence to be actually somewhat faster than what is shown in Figure 9. (Other figures will also be affected, but to a much lesser extent because of their shorter time scale.)

IV. Inversion

The inversion of the data from the momentum, **k**, domain into the coordinate, **r**, domain is discussed in this section. Our ultimate goal for optical pump−diffraction probe experiments is to provide real-time information about the nuclear (and

hopefully one day also electronic) dynamics during the course of chemical reactions. In addition, the $|\Psi(\mathbf{R}, t)|^2$ measurements may be used to compute the potential energy surface on which the atoms are evolving. In a classical mechanical study, Williamson and Zewail have analyzed theoretical transient electron diffraction patterns, giving special attention to the spatial anisotropy induced in the sample by the optical pump pulse[70] and have also fitted their experimental data by assuming that a certain fraction of the molecules in the sample was photoexcited.[58,59] Ewbank et al.[56] have also discussed the inversion of scattering intensities to real space and the computation of the potential energy surface for the case of a diatomic molecule and gas-phase electron diffraction. Their elegant formalism relates the time-dependent intensities to intramolecular potential energy surface parameters and to other parameters taken from spectroscopic investigations, yet it addresses only one electronic surface at a time and it does not simulate the optical excitation stage. (Only least-squares data analysis was used to model experimental data with more than one electronic state.) Our purpose is therefore to complete the quantum modeling of an optical pump−diffraction probe experiment by showing that diffraction intensities from nonstationary samples composed of more than one electronic state can be inverted to recover internuclear distributions and that excited-state dynamics can be isolated using the symmetry of the electronic dipole transition. A hard X-ray wavelength of 56.1 pm (Ag Kα) and a pulse duration of 100 fs (fwhm) are used in all the computations presented in this section (i.e., Figures 10−13).

As is clear from the two-dimensional polar plots of the scattering intensities (Figures 5, 7, and 8), there is both radial and angular information in these gas-phase diffraction intensities. The procedure that we suggest for extracting the radial and angular information from the gas-phase diffraction intensities is motivated by the specific method that we have used to evaluate the nuclear wave function and the diffraction intensity: the wave function was written as a product of an angle-independent radial part and an angular part (which was computed using first- and second-order perturbation theory) and the diffraction intensity as a sum over even products of spherical Bessel functions and Legendre polynomials in the angle between the optical polarization vector and the scattering vector. (In the strong field limit, this approximate procedure for evaluating the nuclear wave function is likely to be less quantitative and a more accurate procedure will have to be used. In such a case, the procedure for inverting the diffraction intensities from the momentum domain to the coordinate domain will have to be modified accordingly.) Our analysis of the diffraction intensities begins with a discussion of the radial information which is then generalized to include the angular information. Before doing so we would like to point out that if the molecular wave function and the diffraction intensity were given in terms of a three-dimensional Cartesian coordinate system, as is likely to be the case for polyatomic systems, we would not try to separate the radial and angular parts but rather invert the diffraction intensity using a three-dimensional Fast Fourier Transform (FFT).

In a stationary isotropic gas-phase sample, the diffraction intensity does not depend on the azimuthal scattering angle and it is given by a sum of two terms: an atomic term (which does not carry any structural information and is given by the sum, over all atoms in the molecules, of the absolute value squared of the atomic structure factors) and a term that is proportional to the zero-order Bessel function, $j_0(sR) = \sin(sR)/sR$, ($l = 0$ term in eq 2.19). The analysis of such an isotropic gas-phase diffraction signal therefore can be done by an inverse sine transform. (To reveal the fine features of the scattering signal, it is customary to first remove the atomic scattering intensity and then analyze the remaining molecular part.) As discussed in the previous section (and in more detail in the Appendix) the diffraction intensity of an anisotropic gas-phase sample can be written as a sum of Bessel functions [$j_l(sR)$ in eq 2.19] that includes all $l \geq 0$ terms with their proper weights, $P_l(\hat{\mathbf{s}}\cdot\hat{\mathbf{e}})$. In this sum, the $l = 0$ term is referred to as the isotropic term, because its weight does not depend on the azimuthal, δ, angle [$P_0(\hat{\mathbf{s}}\cdot\hat{\mathbf{e}}) = 1$]. In a perpendicular arrangement, the weights of all the other $l > 0$ terms depend on both the scattering, α, and azimuthal, δ, angles (cf. eq A.19), and hence they are referred to as the anisotropic part of the diffraction intensity. (In a parallel arrangement, these weights depend only on the scattering angle, α; cf. eq A.18.) To recover the radial part of the wave function, we need to isolate the isotropic term from all the other terms and then analyze it as for an isotropic sample, i.e., via an inverse $j_0(sR)$ transform. If the weights of all the $l > 0$ would not depend on the scattering angle, then an inverse transform of the total intensity would in fact isolate the isotropic term because of the orthonormality of the Bessel functions. However, since the weight of each of the $l > 0$ terms does depend on the scattering angle (i.e., on s), an inverse $j_0(sR)$ transform cannot isolate the isotropic part and as will be shown below it can actually incorporates into it much of the anisotropic part. Thus, to isolate the isotropic part of the diffraction intensity, a more elaborate procedure is required.

To illustrate the procedure that we use, we consider first a simple case where only the $l = 0$ and $l = 2$ terms are included in the expression for the diffraction intensity, eq 2.19. (This is the classical limit of eq 2.19.) In such a case, both the isotropic and anisotropic parts consist of one term whose weight is known at each scattering direction: it equals 1 for the isotropic part and $P_2(\cos\gamma) \equiv P_2[\cos(\alpha/2)\cos\delta]$ for the anisotropic part. If we now consider the diffraction intensity at two different azimuthal angles, δ, but at the same scattering angle, α, then we have a set of two linear equations with two unknowns: the isotropic part and the anisotropic part. (Note that both electronic states, ground and excited, contribute to each of these two terms, isotropic and anisotropic.) By solving this set of equations for the two parts (isotropic and anisotropic) at each scattering angle, α, we can determine both the isotropic part and the anisotropic part. (Again, we emphasize that this procedure does not isolate the ground-state scattering from that of the excited state. What it does is separate the isotropic and anisotropic contributions to the diffraction signal, each of which is composed of both ground- and excited-state terms.) Once we have isolated the isotropic part we can recover the radial part of the wave function by computing its inverse $j_0(sR)$ transform. Again, as is commonly done in the analysis of isotropic gas-phase diffraction signals, the atomic scattering intensity is removed from the isotropic part of the diffraction intensity before the inverse transform is performed. If, as is in general the case, more than two terms are included in eq 2.19, then at each scattering angle, α, a set of N linear equations should be solved, at N different azimuthal angles, to isolate the isotopic part of the diffraction signal. (N is the number of terms that in general will be included in the expression for the total scattering intensity, eq 2.19.) This result implies, as expected, that the higher the resolution that we require (i.e., the more terms we assume contribute to the diffraction signal) the more data (diffraction intensities at different azimuthal angles) we need. In practice, the "classical-like" behavior of the rotational degrees of freedom may allow the isolation of the isotropic part of the diffraction intensity using

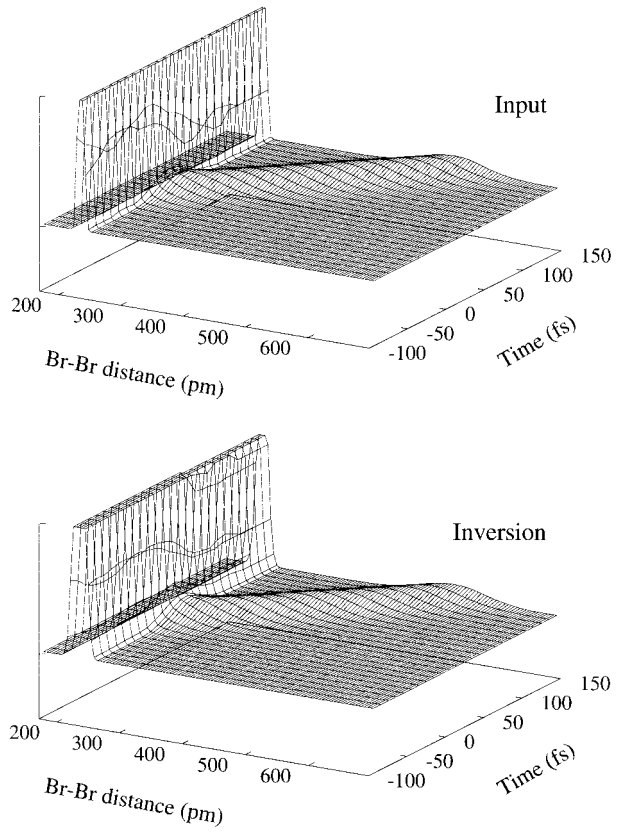

Figure 10. Combined ground- and excited-state densities as a function of internuclear distance and time for molecular bromine. Upper panel: the time-dependent radial part of the electronically incoherent density $n_1(t)|\chi_1(R, t)|^2 + n(t)_2|\chi_2(R, t)|^2$ that is computed numerically and used as an *input* for the computation of the diffraction intensity. Lower panel: the radial distribution function computed by inversion of the time-dependent diffraction intensity (see text for more details on the inversion). In this and all subsequent figures, a hard X-ray wavelength of 56.1 pm (Ag Kα) and an X-ray pulse duration of 100 fs (fwhm) was used in order to achieve this good agreement between the "input" and "output". The constant feature at a short internuclear distance is due to the ground state whereas the time-dependent feature is due to the excited state. Because, compared to the dissociating excited state, the ground state is very localized, its peak magnitude is much larger compared to the dissociating excited state (even though we excite about 26% to the excited state; see inset in Figure 3). Therefore, we truncate the full magnitude of the density, and the decrease in the ground-state density due to the optical excitation is not seen. (In Figure 11 we show the full magnitude of the density and there this decrease is observed.)

the classical limit of eq 2.19. (In this limit, only two terms, $l = 0$ and $l = 2$ contribute to the diffraction intensity.)

This procedure for separating the isotropic part of the diffraction intensity from the total diffraction intensity was applied to both bromine and iodine. Once the isotropic part was isolated, the atomic part was subtracted from it and an inverse $j_0(sR)$ transform was performed on the remaining isotropic molecular part. The result of this procedure is the radial probability density. In Figures 10 and 11, this probability density is compared to the original (radial part of the) quantum mechanical probability density which was used as an input for the computation of the diffraction intensities (eq 2.19, for bromine and iodine, respectively). In both figures, the densities are plotted as a function of internuclear distance (in pm) and time (in fs). (Note that only the electronically incoherent part of the input radial density, $n_1(t)|\chi_1(R,t)|^2 + n_2(t)|\chi_2(R,t)|^2$, is plotted in the upper panels of Figures 10 and 11. This is because, as argued in section III for two well-separated electronic states, the electronically coherent part of the density,

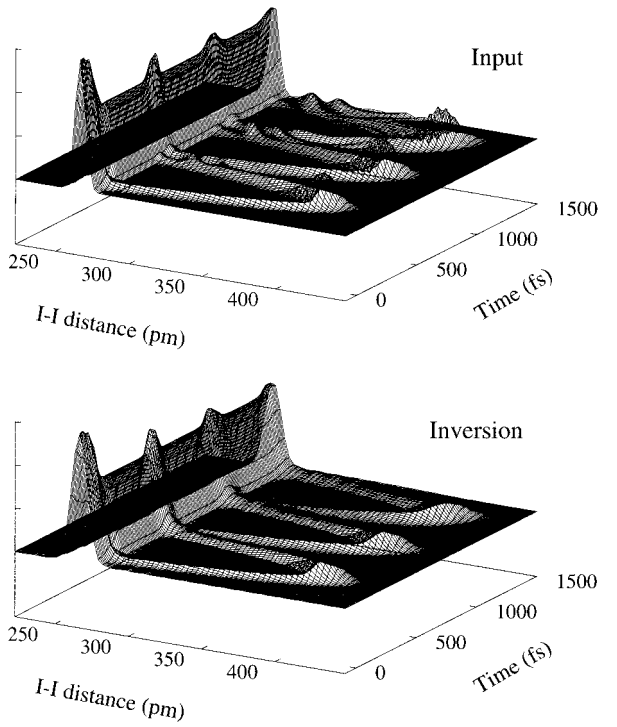

Figure 11. Same as Figure 10, but for molecular iodine. Here we show the full magnitude of the density and therefore the decrease in the ground-state probability due to the optical excitation is very clear. Note the periodic bound vibrational motion of the excited state and the resulting periodic increase in probability at short internuclear distances that occurs whenever the ground and excited states are at similar internuclear distances. Because the excited state is composed of a coherent superposition of high vibrational states (centered about $\nu = 35$), at long times it develops a fine structure (see the upper panel density at long (>1000 fs) delay times) which cannot be resolved with the 56.1 pm (Ag Kα) X-ray wavelength used in this computation.

$C_i^*(t)C_j(t)\chi_i^*(R,t)\chi_j(R,t)$, $i \neq j = 1, 2$, is expected to average to zero upon integration over the time envelope of the diffraction probe pulse.) The agreement between the input quantum dynamics (upper panel in both figures) and the output inversion from diffraction (lower panel in both figures) is very good. The constant feature that appears at short internuclear distances is due to the ground state (in both figures) and in addition there is a time-dependent feature which in Figure 10 is due to the dissociating excited state and in Figure 11 is due to the bound vibrational motion of the excited state. In the case of bromine, Figure 10, we truncate the top of the vertical range of the density on the plot because the ground state is very localized (compared to the excited state) and thus its magnitude is so much larger than that of the dissociating excited state that it would make the latter almost invisible if shown fully on the same scale. Thus, whereas in Figure 11 (where we show the full range of the density) we see both the decrease in the ground-state density (due to the electronic excitation) and the periodic increase in the magnitude of the features at short distances that occurs whenever the ground and excited states are at similar internuclear distances, because of truncation it is not possible to see the decrease in intensity in Figure 10.

We next consider the angular part of the probability density. Given eq 2.19 for the scattering intensity at each scattering angle (α and δ), one can in principle construct numerically the inverse transform that will recover the density as a function of internuclear distance, R, and polar angle, θ. (Note again that this numerical construction of the inverse transform would not be required if the nuclear wave function and the diffraction intensity were given in terms of a three-dimensional Cartesian

coordinate system, in which case a three-dimensional FFT would be used to invert the data.) This inverse transform is much more complicated than the simple inverse ($l = 0$) sine transform that is used in the analysis of isotropic gas-phase diffraction intensities because it includes higher ($l > 0$) Bessel functions and because these Bessel functions are weighted by Legendre polynomials [$P_l(\hat{\mathbf{s}}\cdot\hat{\mathbf{e}})$] that depend on the scattering angle α. However, it is important to note that this transform does exist and therefore, in principle, one can recover the density as a function of internuclear density and polar angle θ. [Because of the symmetry of our system, the distribution of **R** is independent of φ, so that we need only to recover $\rho(R, \theta)$ from the two-dimensional diffraction intensity.] Since the numerical transformation described above is so complicated, we try to recover the angular information by a much simpler procedure: a simple inverse $j_0(sR)$ transform of the scattering intensity at each azimuthal angle δ. (Note that the angular dependence of the diffraction intensity on the azimuthal angle δ is similar to the angular dependence of the wave function on the polar angle θ; i.e., $\delta \rightarrow \theta$.) As argued above, although the Bessel functions are orthonormal, an inverse $j_0(sR)$ transform does *not* isolate the isotropic part of the diffraction intensity because the weights of all $l > 0$ Bessel functions that contribute to the total diffraction intensity depend on the scattering angle. Thus, an inverse $j_0(sR)$ transform will reflect both the isotropic and the anisotropic parts of the diffraction intensity (although not in an exact way). For not too long pump−probe delay times, the initial alignment will be retained and thus, in a polar representation, we expect to see the excited-state internuclear axes aligned preferentially along the electric vector direction of the light, for this parallel transition, whereas the opposite is true for the ground state, which is expected to be depleted in this direction. In Figure 12, we show polar representations of the two-dimensional probability density, $\rho(R, \theta)$, at a series of increasing pump−probe delay times for molecular iodine. In these polar plots, the distance from the origin to a point on the graph is the internuclear distance (in pm) and the angle between this distance and the vertical axis is the polar angle θ. Three of the panels show the result of the inversion procedure (at three points in time during the first vibrational period on the excited electronic state), and in the third panel (from the top) we show, for comparison, the input density at one point in time. Although we have used an approximate procedure for the inversion, the agreement between the input and the output is quite good. The time-dependent features in these polar plots are mainly due to the bound vibrational motion on the excited electronic state, which is preferentially aligned along vertical *Z* axis. The ground state is depleted in this direction and is aligned predominantly (although not completely because only ∼15% of the ground-state population is excited) along the *X* axis. After 245 fs from the electronic excitation (two middle panels), the excited electronic state is at an outer turning point and it is thus more localized than at 80 fs (upper panel). At 495 fs (lower panel), the ground- and excited-state densities are at very similar distances and therefore we see basically a single feature with only traces of angular asymmetry. (The dashed contour line is drawn at a value that is 45 times lower than the highest one, which is the innermost contour.)

Finally, we discuss how to use the difference in the ground- and excited-state dynamics and symmetry of the electronic dipole transition in order to isolate the excited-state dynamics from the ground-state dynamics. From Figure 12 it is clear that at early times the excited-state density is aligned along the polarization direction *Z*, whereas there is practically no density in the direction perpendicular to it.[70] This implies that if we take the difference between the density along the parallel and perpendicular directions (after properly normalizing them according to the peak that appears in both directions and therefore can be assumed to be due to the ground state), we should recover the excited state alone. As an example, this procedure is applied to the diffraction intensity of iodine 245 fs after the optical excitation. In the upper panel of Figure 13, we plot a slice of Figure 12 (second panel from top) along the *Z* direction where we see both the ground and the excited states. In the middle panel of Figure 13, we plot another slice of Figure 12 but this

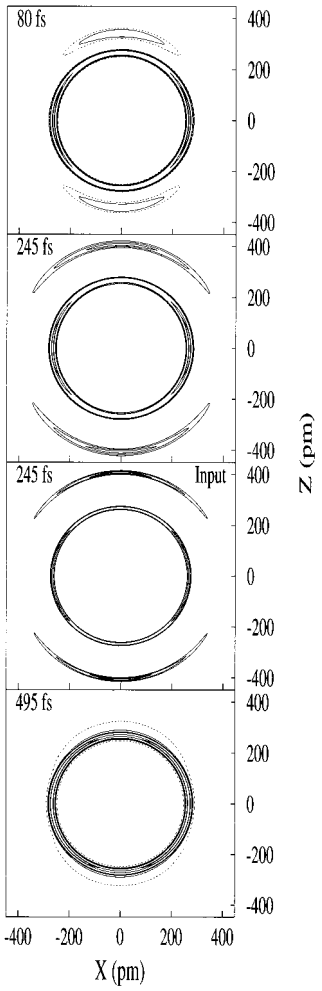

Figure 12. A polar representation of the I_2 probability density, $\rho(R, \theta)$, computed by inversion of the time-dependent diffraction intensity, at a series of increasing pump−probe delay times. (The three "snapshots" that we show are during the first vibrational period on the excited electronic state.) The distance from the origin to a point on the graph is the I−I internuclear distance, and the angle between this distance and the vertical *Z* axis is the polar angle θ. The full contours are drawn at values of 0.1, 0.2, 0.3, 0.8, and 0.9, and the dashed ones are at 0.075 (uppermost panel) and 0.02 (lowermost panel). The time-dependent features that are due to the excited-state bound vibrational dynamics are aligned predominantly along the *Z* axis (as expected for a parallel transition) and the ground state (features at internuclear distances of ∼266 pm) is depleted in this direction. Note that because the transition probability is not unity (but rather ∼15%), after the excitation the ground state is preferentially aligned perpendicular to the optical polarization direction but it is not completely depleted along the direction of the electronic excitation and that when the ground and excited states are at similar internuclear distances (lowest panel) we see a single feature that is almost isotropic. For comparison, in the third panel from the top, we also show (at one point in time) the three-dimensional input density (incoherently averaged over the initial *J*, *M* distribution) used as an input for the computation of the diffraction intensity.

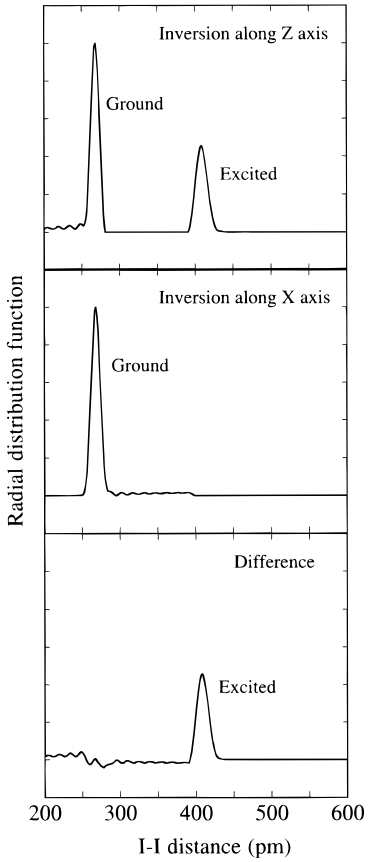

Figure 13. Upper panel: a slice of the iodine distribution function shown in the second panel (from the top) of Figure 12 along the light polarization direction (vertical *Z* axis). Middle panel: same as upper panel but this time along the perpendicular direction (*X* axis) where at short pump−probe delay times (compared to the rotational delocalization time) there are no traces of the excited electronic state. To isolate the excited state, the upper two panels were normalized using the area under the constant feature which is assumed to be due to the stationary ground state. Lower panel: the difference between the upper and middle panels, showing that the excited-state internuclear distribution can be isolated from the diffraction data by symmetry. Note that, as discussed in the text, when the ground- and excited-state wave functions are at similar internuclear distances, such a simple procedure will not enable us to really isolate the excited state from the ground state but only to conclude that the two states are at similar internuclear separations.

time along the perpendicular *X* direction where there are practically no traces of the excited state at short times (at longer times after the pump pulse we do expect to see again a mixture of both states due to rotational delocalization). Once we subtract the two results (after normalizing them so that the peak that appears in both panels has the same area), we isolate the ground state, shown in the lower panel of Figure 13. We have applied this procedure, using the symmetry of the electric dipole transition, for both iodine and bromine at various pump−probe delay times and our experience is that in the weak field limit it is a quite robust way to separate the short-time excited-state dynamics from those of the ground state. [Of course, it will not be always possible to *separate* the two states because when the ground and excited states are at very similar internuclear distances we will see only a single peak in the distribution in both directions (parallel and perpendicular, cf. Figure 12) and thus will only be able to conclude that the ground and excited states are at similar internuclear distances.] Since, even for polyatomic molecules there still exists a molecule-fixed electronic transition dipole, it will be interesting to try and extend this procedure to more complex molecules.

V. Concluding Remarks

In this paper we have discussed a natural development of stationary X-ray and electron diffraction experiments: time-dependent measurements of nonstationary transient structures. The experimental scheme that has been proposed to enable the direct measurement of evolving structures is ultrafast X-ray and electron diffraction. In such experiments, the sample and the pump and probe pulses are all time-dependent and the general theory presented in section III.A accounts for these features. Unlike previous theoretical derivations of optical pump−diffraction probe experiments, our formalism treats both the electronic and nuclear degrees of freedom quantum mechanically, and it models the ultrafast optical pump process, the subsequent quantum dynamics of the sample, and the ultrafast diffraction probe process. With electronic excitation by the pump pulse, more than one electronic state will usually contribute to the measured diffraction intensity, and interferences between ro-vibrational states involving different electronic states and ro-vibrational interferences within a given electronic state appeared explicitly in the expression for the instantaneous X-ray and electron scattering intensity (cf. eq 2.12 or 2.17). Since the duration of currently available X-ray or electron pulses is still long when compared to the period of the frequency associated with the energy difference between two well-separated electronic states, we assumed that interference between different electronic states averages to zero (upon time integration over the envelope of the field intensity) so that the time-integrated scattering intensity is given by a sum of the individual electronic-state scattering intensities, weighted by the appropriate fractional populations (eqs 2.14 and 2.15). This result has been assumed in all previous gas-phase electron diffraction studies, and although we have used it in the present computations, we would like to emphasize that this is an approximation that will break down when electronic surfaces approach one another, for example, in curve crossing, and more generally whenever the duration of the probe X-ray or electron pulse is comparable to the period associated with the energy difference between two electronic states. In addition, the common assumption we have made here that the observed scattering is inelastic with respect to the nuclear degrees of freedom and elastic with respect to the electronic degrees of freedom is a simplification which needs to be considered more deeply, with respect to electron diffraction versus X-ray diffraction in general, and to time-dependent phenomena in particular.

Two numerical examples were discussed in section III: the dissociative and bound gas-phase dynamics for diatomic molecules. (The parallel case for a crystal, involving electronic excitation and phonon nuclear dynamics could also be carried out.) It is shown that, with the scattering involving both ground- and excited-state molecules, significant changes are observed in the time-dependent X-ray diffraction pattern. These results suggest that molecular, and in particular dissociative, dynamics may be used to measure the duration of sub-picosecond X-ray or electron pulses with time resolution of tens of femtoseconds. As expected, the changes in diffraction intensity are less pronounced whenever the ground- and excited-state wave packets are at similar internuclear distances and even more so if the wave packets are also delocalized. The computation of the time-dependent molecular wave function is approximated by dividing it into two parts by writing the wave function as a product of an angle-independent radial part and an angular part, both being time dependent. The former is computed numerically (by solving the radial time-dependent Schrödinger equation); the latter is evaluated analytically in the Appendix (using first- and second-order perturbation theory for the excited and ground

states, respectively). Apart from reducing the computational difficulty, this approximation enables us to analytically recover the known[15,16,57,70] breaking of cylindrical symmetry in gas- and liquid-phase diffraction patterns that is expected whenever the direction of the optical polarization (which is the only symmetry axis in the sample after the optical excitation) does not coincide with the direction of the incident X-ray (or electron) beam. As discussed in section III (and in more detail in the Appendix), the total diffraction intensity for an anisotropic gas-phase sample can be written as a sum of Bessel functions [$j_l(sR)$ in eq 2.19] weighted by Legendre polynomials, $P_l(\hat{\mathbf{s}}\cdot\hat{\mathbf{e}})$. Since the latter depends on the scattering angle, a simple inverse $j_0(sR)$ transform *cannot* isolate the isotropic part of the diffraction intensity, and in section IV we have suggested and applied an exact procedure for separating the isotropic part of the diffraction pattern from the total diffraction pattern. This procedure enabled us to recover (very nicely) the radial part of the wave function as a function of time. Although we have discussed the exact procedure for recovering the angular dependence of the probability density, in this paper we have only used an approximate procedure to recover it. [The proposed approximate procedure was based on the observation that an inverse $j_0(sR)$ transform cannot isolate the isotropic part of the diffraction intensity (because of the s dependence of the weights of the Bessel functions), and therefore, if that transform is used to invert the total diffraction intensity, the resulting inverted density can have a nonisotropic contribution.] This approximate procedure enabled us to demonstrate how the short-time excited-state dynamics can be isolated from that of the ground state using the symmetry induced by the electronic dipole transition. (At short times, the exact procedure for inverting the two-dimensional diffraction intensity could also be used to isolate the excited-state dynamics from that of the ground state.)

Since our discussion in section III was limited to diatomic molecules, we were able to compute the nuclear dynamics quantum mechanically. This will not be possible for any but the smallest polyatomic systems, and other computationally less demanding methods will have to be used. We believe that, to correctly model optical pump−diffraction probe experiments, these methods will have to retain some quantum mechanical features (such as the notion of more than one electronic state and phase interferences, for example).

Throughout most of this paper (and in all our numerical examples) we limited our discussion to the independent atom model. Within the limits of this model, the electronic cloud is not allowed to deform as the atoms and molecules are moving. Thus, the time dependence of the diffraction intensities was associated only with the nuclear motion (or, in other words, with the spherical core electronic cloud) and did not reflect bonding changes in valence electrons. Such an approximation limits the discussion to changes in bond distances and angles and cannot account for the electron dynamics. Although it is not expected that initial ultrafast diffraction measurements will be of sufficient accuracy to observe the dynamics of the relatively few bonding electrons, the evolution of the electron density during the course of a chemical reaction is a basic part of our understanding of the making, altering, and breaking of chemical bonds, and we do believe that ultrafast diffraction (X-ray and electron) may in time enable the direct imaging of electronic (as well as nuclear) dynamics.

Acknowledgment. The authors thank Dr. J. Che, F. Ráksi, and Prof. P. M. Weber for many helpful discussions. M.B.N. thanks the Rothschild Foundation for a Postdoctoral Fellowship and the United States−Israel Educational Foundation for a Fulbright Postdoctoral award.

Appendix: Rotational Dynamics

In this appendix we treat the rotational part of the quantum dynamics for electron and X-ray diffraction from a gas-phase diatomic sample pumped by a linearly polarized light pulse. As discussed in section II (eq. 2.6), the molecular wave function, $\Psi_j(\mathbf{r}, \mathbf{R}, t)$, on each electronic state j is written as a product of an electronic part, $\phi_j(\mathbf{r}; \mathbf{R})$, and a time-dependent nuclear part, $\chi_j(\mathbf{R}, t)$, such that

$$\Psi_j(\mathbf{r}, \mathbf{R}, t) = C_j(t)\phi_j(\mathbf{r}; \mathbf{R})\chi_j(\mathbf{R}, t) = C_j(t)\phi_j(\mathbf{r}; \mathbf{R})\sum_\nu d_j^\nu(t)\chi_j^\nu(\mathbf{R}) \quad \text{(A.1)}$$

in which ν implies a summation over vibrational and rotational indices, and $\chi_j^\nu(\mathbf{R})$ is a nuclear eigenstate. In this appendix we discuss the computation of the angular part of the nuclear wave function for the illustrative specific case of a gas-phase diatomic molecule, noting that the electronic part is assumed to be known (i.e., the potential energy surfaces are given as an input) and that the radial part (which, as is often done for computational simplicity, is assumed to be independent of J) is computed numerically (see section III.A for more details). In addition, we show how to evaluate the integral needed to calculate the scattering intensity from the wave function.

Since the computation of rotational selection rules and transition line strength is well documented in the literature,[85,87] we try to make the discussion as short as possible and center attention only the details that are specific to the diffraction probing scheme or to any approximation that we make. The purpose of the somewhat tedious procedure that we outline is to (i) provide an analytical expression for the rotational part of the molecular wave function and (ii) use this expression to reduce the three-dimensional Fourier transform needed for the scattering intensity (cf. eq 2.18) to a one-dimensional transform, in the radial coordinate, multiplied by an analytic expression. Although the procedure is rather long, and it is dictated by the fact that we use a polar coordinate system and numerically evaluate only the radial part, the analytical result that we obtain does provide a quantum insight to the breaking of symmetry in the diffraction pattern, which has been previously discussed classically.[15,16,70]

We first rewrite the nuclear wave function (of each electronic state) as a product of a radial part, $\chi_j(R, t)$, and an angular part, $Y_j(\theta, \varphi, t)$,

$$\Psi_j(\mathbf{r}, \mathbf{R}, t) = C_j(t)\phi_j(\mathbf{r}; \mathbf{R})\chi_j(R, t)Y_j(\theta, \varphi, t) \quad \text{(A.2)}$$

[The polar angle θ is the angle between the internuclear vector $\mathbf{R}$ and the lab frame Z axis, and the azimuthal angle φ is the projection (with respect to the X axis) of the internuclear vector on the XY plane.] In principle, both the radial and the angular wave functions are given by a sum over vibrational and rotational eigenfunctions. Thus, within each electronic state, the rotational eigenfunctions depend on the vibrational level and due to the nature of the electronic excitation there will be more than one occupied vibrational state on the excited electronic state. Here we make an approximation whose character is dictated by the specific procedure used to compute the radial part. Since in practice we generate a single radial wave packet (which is assumed to be independent of J) and we do not decompose it into vibrational eigenstates, we assume that the rotational part carries a single vibrational (or more precisely

radial) index which is determined by the central vibrational eigenstate in the wave packet. For the heavy diatomic molecules in the specific cases discussed in section III and for not too long pump−probe delay times, this approximation is quite good for the rotational dynamics, because of the very long rotational period and the relatively weak dependence of the rotational constant on the vibrational state, over the vibrational range excited. Within this approximation, the angular wave function can be written as a sum over rotational eigenstates ($|J'\ K'\ M'\rangle$)

$$Y_j(\theta, \varphi, \chi, t) = \sum_{J',K',M'} a(J, K, M, J', K', M')|J'\ K'\ M'\rangle \exp(i\omega_j^n t) \quad \text{(A.3)}$$

and, as discussed above, we associate a single "vibrational" index, n, that corresponds to the central vibrational eigenstate of the radial wave packet, to the rotational part. In eq A.3, we follow the conventional notation used in the literature[87] by associating Λ (the molecule fixed electronic component of the total angular momentum, J, along the internuclear axis) of a diatomic molecule with K of an asymmetric top molecule, and the rotational frequency $\omega_j^n = B_n J(J+1)$, where $B_n = B_e - \alpha_e(n + {}^1/_2)$ in which B_e is the rotational term corresponding to the equilibrium bond length and α_e is a small positive number that accounts for the coupling between the rotation and vibration of the molecule. Each of the rotational states ($|JKM\rangle$) in eq A.3 can be written using rotation matrices:[85,86]

$$|JKM\rangle = (-1)^{M-K}\left(\frac{2J+1}{8\pi}\right)^{1/2} D^J_{-M-K}(\theta, \varphi, 0) \quad \text{(A.4)}$$

After the interaction with polarized light, the excited state becomes a coherent superposition of rotational (and vibrational) states and the ground electronic state is partially coherent: the polarized pump pulse creates a "hole" in the initial isotropic ground-state distribution. What we would like to know are the amplitudes of these states (i.e., the a factors in eq A.3), assuming a single-photon process. (Note that this is only an assumption and not an exact result because cycling between the two electronic states can result in a tighter rotational distribution than the one predicted here.[83]) We first consider the excited state. The probability amplitude of finding the excited-state rotor in a $|J'\ K'\ M'\rangle$ state following the dipole absorption of linearly polarized light [and assuming (A.4) as the initial ground rotational state] is given by the Clebsch−Gordan coefficient,

$$\langle J'\ K'\ M'|\Phi_{Fg}|JKM\rangle \quad \text{(A.5)}$$

where Φ_{Fg} is the so-called direction cosine matrix.[87] For light polarized along the Z axis (in the lab frame) and for a parallel transition (i.e., the molecular dipole transition is along the internuclear axis, z), $\Phi_{Fg} = \Phi_{Zz} = \cos\theta$, which is the projection of the molecular transition dipole on the lab frame Z axis. In a perpendicular transition, the molecular dipole is in the $x-y$ plane and hence one should use $\Phi_{Fg} = \Phi_{Zx} + \Phi_{Zy} = -\sin\theta\cos\chi + \sin\theta\cos\chi$.[87] (The spin angle χ should not be confused with the molecular wave function.) Integrals of the form (A.5) can be solved analytically by writing the direction cosine matrix (as well as the rotational eigenfunction, eq A.4) in terms of rotation matrices and using the Clebsch−Gordan series to evaluate the resulting integrals over three rotational matrices. Since these integrals appear in many text books (see, for example, chapter 2 in ref 87), here we only write the direction cosine matrix in terms of rotation matrices,

$$\Phi_{Zz} = D^1_{00}$$

$$\Phi_{Zx} = \frac{1}{\sqrt{2}}(D^1_{0-1} - D^1_{01})$$

$$\Phi_{Zy} = \frac{i}{\sqrt{2}}(D^1_{01} + D^1_{0-1}) \quad \text{(A.6)}$$

The equivalent expression for the rotational wave function is given by eq A.4. Thus, for example, if the ground state is initially given by eq A.4 and the transition is parallel, then the angular part of the excited state ($j = 2$) is given by

$$Y_2(\theta, \varphi, t) = a(J0M, J+1, 0M)|J+1, 0, M\rangle \exp(i\omega^n_{J+1}t) + a(J0M, J-1, 0M)|J-1, 0, M\rangle \exp(i\omega^n_{J-1}t) \quad \text{(A.7)}$$

where we have assumed the usual case for the ground-state diatomic molecule, $K \equiv \Lambda = 0$. i.e., it is of Σ (or $\Omega = 0$) electronic symmetry. The values of the coefficients in eq A.7 are determined by eq A.5 using the uppermost equation in (A.6).

We now discuss the angular wave function of the ground state, $Y_1(\theta, \varphi, \chi, t)$. First note that the orthogonality of the electronic wave functions and the chosen normalization of the radial part of the wave function imply that

$$\langle\Psi(\mathbf{r}, \mathbf{R}, t)|\Psi(\mathbf{r}, \mathbf{R}, t)\rangle = n_1\langle\chi_1|\chi_1\rangle\langle Y_1|Y_1\rangle + n_2\langle\chi_2|\chi_2\rangle\langle Y_2|Y_2\rangle = n_1\langle Y_1|Y_1\rangle + n_2\langle Y_2|Y_2\rangle = 1 \quad \text{(A.8)}$$

in which the last equality is due to norm conservation. (Note that during the electronic excitation the ground- and excited-state populations vary as a function of time.) As discussed in detail above (for a single-photon process), the excited-state wave function is given by the result of the dipole operator on the initial ground rotational state, $Y_2 = \Phi_{Fg}|JKM\rangle$ and therefore,

$$n_1\langle Y_1|Y_1\rangle = \langle JKM|(1 - n_2\Phi^*_{Fg}\Phi_{Fg})|JKM\rangle \quad \text{(A.9)}$$

In which n_j is the fractional population of the jth electronic state. Since we need to know the ground-state amplitude, Y_1, we take the square root of eq A.9 and, keeping only linear terms in the excited-state fractional population, write

$$\sqrt{n_1}|Y_1\rangle \approx \left(1 - \frac{n_2}{2}\Phi^*_{FG}\Phi_{Fg}\right)|JKM\rangle \quad \text{(A.10)}$$

Physically what eq A.10 implies is that the ground-state distribution is derived using second-order perturbation theory (or alternatively first-order perturbation theory applied twice) and that after the electronic excitation the initially isotropic ground state becomes an anisotropic linear superposition of the original state and any state that can be accessed via a two-photon process (absorption and emission) given the appropriate selection rules. Hence, the amplitude for finding the ground state in a $\langle J'\ K'\ M'|$ state after the interaction with linearly polarized light is computed just as for the excited state: i.e., by bracketing the left-hand side of eq A.10 with a $\langle J'\ K'\ M'|$ state; cf. eq A.5. We then write both the initial and the final states, as well as the square of the dipole operator, $\Phi^*_{Fg}\Phi_{Fg}$, in terms of rotation matrices, eq A.6, and use the Clebsch−Gordan series to analytically evaluate the amplitudes. The end result for the ground state is somewhat more complicated than for the excited state (this is particularly so for a perpendicular transition) and its general form is given by eq A.3.

Once the angular parts of both the ground and the excited states have been determined (analytically) and the radial part computed numerically, we still need to evaluate three-

dimensional integrals of the form (cf. eq 2.18 in text)

$$2n_j\langle Y_j(\theta, \varphi, t)\chi_j(R, t)|1 + \cos(\mathbf{s}\cdot\mathbf{R})|\chi_j(R, t)Y_j(\theta, \varphi, t)\rangle, \quad j = 1, 2 \quad \text{(A.11)}$$

in order to compute the diffraction intensity from the wave function.

In what follows, we rewrite these integrals as a product of a radial part and an angular part and evaluate the latter analytically, thereby reducing the dimensionality of the numerical integration from three to one. This is done by expanding the $\cos(\mathbf{s}\cdot\mathbf{R})$ in eq A.11 in terms of products of even Bessel functions, $j_l(sR)$, and Legendre polynomials, $P_l(\cos\beta)$,

$$\cos(\mathbf{s}\cdot\mathbf{R}) = \sum_{l=0}^{\infty}(\pm i)^l j_l(sR)(2l + 1)P_l(\cos\beta) \quad \text{(A.12)}$$

in which, $\cos\beta = \hat{\mathbf{s}}\cdot\hat{\mathbf{R}}$ is the angle between the scattering vector $\mathbf{s}$ and the internuclear vector $\mathbf{R}$, the $\hat{}$ symbol is used to denote a unit vector, and only even l terms contribute to the sum. Using the addition theorem,[97] the Legendre polynomials are written in terms of spherical harmonics

$$(2l + 1)P_l(\cos\beta) = 4\pi\sum_{m=-l}^{m=l} Y_l^m(\hat{\mathbf{R}})Y_l^{m*}(\hat{\mathbf{s}}) \quad \text{(A.13)}$$

The $\Delta m = 0$ selection rule (for the electronic transition) implies that only $m = 0$ terms in this expansion should be considered, for which one can write

$$Y_l^0(\hat{\mathbf{R}}) = Y_l^0(\theta) = \left(\frac{2l + 1}{4\pi}\right)^{1/2} P_l(\hat{\mathbf{R}}\cdot\hat{\mathbf{Z}})$$

$$Y_l^0(\hat{\mathbf{s}}) = \left(\frac{2l + 1}{4\pi}\right)^{1/2} P_l(\hat{\mathbf{s}}\cdot\hat{\mathbf{Z}}) \quad \text{(A.14)}$$

by letting the lab frame Z axis coincide with the molecular z axis. Note that the unit vector in the Z direction is the polarization direction, $\hat{\mathbf{e}}$, and therefore, using eqs A.14 and A.13 we can rewrite eq A.12 as

$$\cos(\mathbf{s}\cdot\mathbf{R}) = \sum_{l=0}^{\infty}(\pm i)^l j_l(sR)4\pi\left(\frac{2l + 1}{4\pi}\right)^{1/2} P_l(\hat{\mathbf{s}}\cdot\hat{\mathbf{e}})Y_l^0(\theta) \quad \text{(A.15)}$$

Equation A.15 enables us to invoke the Clebsch−Gordan theorem again and evaluate analytically the integral over three spherical harmonics [two from the angular part of the nuclear wave function, eq A.13, and one from the expansion of $\cos(\mathbf{s}\cdot\mathbf{R})$, eq A.15]. Thus, using the expansion in eq A.15 and eq A.2 for the molecular wave function, we can write the time integrated scattering intensity as

$$I_j(\mathbf{s}, \tau) = 2\int_{-\infty}^{+\infty} dt A(t, \tau)n_j(t)|f_j(s)|^2\left[1 + \sum_{l=0}^{\infty}(i)^l 4\pi\sqrt{\frac{2l + 1}{4\pi}}P_l(\hat{\mathbf{s}}\cdot\hat{\mathbf{e}})\Xi_l(t)\langle\chi_j(R, t)|j_l(sR)|\chi_j(R, t)\rangle\right] \quad \text{(A.16)}$$

where

$$\Xi_l(t) = \langle Y_j(\theta, \varphi, t)|Y_{l0}(\theta, \varphi)|Y_j(\theta, \varphi, t)\rangle \quad \text{(A.17)}$$

The one-dimensional radial part $[\langle\chi_j(R, t)|j_l(sR)|\chi_j(R, t)\rangle$ in eq A.16] is computed numerically, and this procedure is repeated for both electronic states ($j = 1, 2$) at any point in time for which we compute the diffraction pattern. (We reiterate that because of the even symmetry in our problem only even l terms contribute to the sum in eq A.16.) The Clebsch−Gordan theorem determines that the upper bound on the infinite sum in eq A.17 equals $(2J + 2)$, where J is the initial rotational eigenstate on the ground electronic state. In the classical limit (of high J), only two terms, $l = 0$ and 2, contribute to the sum in eq A.16.

The angles between the optical polarization vector, $\hat{\mathbf{e}}$, and the scattering vector, $\hat{\mathbf{s}}$, do not depend on the azimuthal scattering angle δ (see Figure 2, lower panel) when the incident X-ray (or electron) beam and the polarization vector are parallel

$$\cos\gamma = \hat{\mathbf{s}}\cdot\hat{\mathbf{e}} = \sin(\alpha/2) \quad \text{(A.18)}$$

whereas it does when they are perpendicular (incoming beam is along the X direction for example; cf. upper panel in Figure 2)

$$\cos\gamma = \cos(\alpha/2)\cos\delta \quad \text{(A.19)}$$

In eqs A.18 and A.19, α is the angle between the incident and scattered X-rays or electrons and δ is its azimuthal projection on the detector plane (see Figure 2). Thus, it is clear that in the perpendicular arrangement, eq A.19, the diffraction intensity will not be symmetrical with respect to rotation of δ about the axis of the incoming X-ray or electron beam whereas it will be in the parallel arrangement. In the main text we elaborate on this point in more detail.

Finally, we note (as discussed in section II.B) that the ground- and excited-state angular distributions and the resulting diffraction intensity should be computed (using the procedure outlined in this appendix) for each of the ground rotational states that is initially populated. The total scattering intensity, for an initially thermal sample, is given by a Boltzmann average of these individual diffraction intensities (each of which corresponds to a given initial ground rotational state).

References and Notes

(1) Glusker, J. P.; Trueblood, K. N. *Crystal Structure Analysis*; Oxford University Press: New York, 1972.

(2) Stout, E. G.; Jensen, L. H. *X-ray Structure Determination, A Practical Guide*; Macmillan: New York, 1968.

(3) *Fifty Years of Electron Diffraction*; Goodman, P., Ed.; Reidel: Dordrecht, The Netherlands, 1981.

(4) *Stereochemical Applications of Gas-Phase Electron Diffraction*; Methods in Stereochemical Analysis 1; Hargittai, I., Hargittai, M., Eds.; VCH: New York, 1988.

(5) Rhodes, G. *Crystallography Made Crystal Clear*; Academic Press: San Diego, 1993.

(6) Fleming, G. R. *Chemical Applications of Ultrafast Spectrospcopy*; Oxford University Press: New York, 1986.

(7) *Time-Resolved Electron and X-ray Diffraction*; SPIE Proceedings Series 2521; Rentzepis, P. M., Ed.; SPIE: Bellingham, WA, 1995.

(8) Wark, J. *Contemp. Phys.* **1996**, *37*, 205.

(9) *Time Resolved Electron and X-ray Diffraction*; Rentzepis, P. M., Helliwell, J., Eds.; Oxford University Press: New York, in press.

(10) Williamson, J. C. *Chem. Phys. Lett.* **1993**, *209*, 472.

(11) Johnson, Q.; Keeler, R. N.; Lyle, J. W. *Nature* **1967**, *213*, 1114.

(12) Johnson, Q.; Mitchell, A. C.; Keeler, R. N.; Evans, L. *Phys. Rev. Lett.* **1970**, *25*, 1099.

(13) Johnson, Q.; Mitchell, A. C. *Phys. Rev. Lett.* **1972**, *29*, 1369.

(14) Johnson, Q.; Mitchell, A. C.; Smith, I. D. *Rev. Sci. Instrum.* **1980**, *51*, 741.

(15) Bado, P.; Berens, P. H.; Bergsma, J. P.; Coladonato, M. H.; Dupuy, C. G.; Edelsten, P. M.; Kahn, J. D.; Wilson, K. R.; Fredkin, D. R. *Laser Chem.* **1983**, *3*, 231.

(16) Bergsma, J. P.; Coladonato, M. H.; Edelsten, P. M.; Wilson, K. R.; Fredkin, D. R. *J. Chem. Phys.* **1986**, *84*, 6151.

(17) Van Wonterghem, B.; Rentzepis, P. M. *App. Phys. Lett.* **1990**, *56*, 1005.

(18) Anderson, T.; Tomov, I. V.; Rentzepis, P. M. *J. App. Phys.* **1992**, *71*, 5161.

(19) Tomov, I. V.; Anderson, T.; Rentzepis, P. M. *J. X-ray Sci. Technol.* **1993**, *4*, 44.
(20) Anderson, T.; Tomov, I. V.; Rentzepis, P. M. *J. Chem. Phys.* **1993**, *99*, 869.
(21) Tomov, I. V.; Chen, P.; Rentzepis, P. M. *Exp. Technol. Phys.* **1994**, *40*, 165.
(22) Tomov, I. V.; Chen, P.; Rentzepis, P. M. *Rev. Sci. Instrum.* **1995**, *66*, 5214.
(23) Tomov, I. V.; Chen, P.; Rentzepis, P. M. In *Time-Resolved Electron and X-ray Diffraction*; Rentzepis, P. M., Ed. *Proc SPIE-Int. Soc. Opt. Eng.* **1995**, *2521*, 13.
(24) Chen, P.; Tomov, I. V.; Rentzepis, P. M. *J. Chem. Phys.* **1996**, *104*, 10.
(25) Forsyth, J. M.; Frankel, R. D. Flash X-ray Diffraction from Biological Specimens Using a Laser Produced Plasma Source: A Progress Report. Laboratory for Laser Energetics, University of Rochester, Rochester: New York, 1980.
(26) Frankel, R. D.; Forsyth, J. M. In *Methods in Enzymology;* Packer, L., Ed.; Academic Press: New York, 1982.
(27) Wark, J. S.; Whitlock, R. R.; Hauer, A. A.; Sawin, J. E.; Solone, P. J. *Phys. Rev. B* **1987**, *35*, 9391.
(28) Murnane, M. M.; Kapteyn, H. C.; Falcone, R. W. *Phys. Rev. Lett.* **1989**, *62*, 155.
(29) Kmetec, J. D.; Gordon, C. L., III; Macklin, J. J.; Lemoff, B. E.; Brown, G. S.; Harris, S. E. *Phys. Rev. Lett.* **1992**, *68*, 1527.
(30) Sher, M. H.; Mohideen, U.; Tom, K. H. W.; Wood, O. R., II; Aumiller, G. D.; Freeman, R. R.; McIlrath, T. J. *Opt. Lett.* **1993**, *18*, 646.
(31) Maksimchuk, A.; Workman, J.; Liu, X.; Ellenberger, U.; Coe, S.; Chien, C.-Y.; Umstadter, D. In *X-ray Lasers*; Eder, D. E., Matthews, D., Eds.; American Institute of Physics: New York, 1994; Vol. 332.
(32) Rousse, A.; Audebert, P.; Geindre, J. P.; Fallies, F.; Gauthier, J. C.; Mysyrowicz, A.; Grillou, G.; Antonetti, A. *Phys. Rev. E* **1994**, *50*, 2200.
(33) McPherson, A.; Thompson, B. D.; Borisov, A. B.; Boyer, K.; Rhodes, C. K. *Nature* **1994**, *370*, 631.
(34) Svanberg, S.; Larsson, J.; Persson, A.; Wahlstrom, C.-G. *Phys. Scr.* **1994**, *49*, 187.
(35) Schins, J. M.; Breger, P.; Agostini, P.; Constantinescu, R. C.; Muller, H. G.; Grillon, G.; Antonetti, A.; Mysyrowicz, A. *Phys. Rev. Lett.* **1994**, *73*, 2180.
(36) Deleted in proof.
(37) Ráksi, F.; Wilson, K. R.; Jiang, Z.; Ikhlef, A.; Côté, C. Y. and Kieffer, J.-C. In *Applications of Laser Plasma Radiation II, Proc. SPIE-Int. Soc. Opt. Eng.* **1995**, *2523*, 306.
(38) Ráksi, F.; Wilson, K. R.; Jiang, Z.; Ikhlef, A.; Côté, C. Y.; Kieffer, J.-C. *J. Chem. Phys.* **1996**, *104*, 6066.
(39) Jiang, Z.; Ikhlef, A.; Kieffer, J.-C.; Ráksi, F.; Wilson, K. R. In *Ultrafast Phenomena X*; Fujimoto, J., Zinth, W., Barbara, P. F., Knox, W. H., Eds.; Springer-Verlag: Berlin, 1996; Vol. 62, p 274.
(40) Guo, T.; Raksi, F.; Rose-Petruck, C.; Squier, J.; Walker, B.; Weber, P. M.; Wilson, K. R. and Barty, C. P. J., unpublished.
(41) Srajer, V.; Teng, T.-y.; Ursby, T.; Pradervand, C.; Ren, Z.; Adachi, S.-i.; Schildkamp, W.; Bourgeois, D.; Wulff, M.; Moffat, K. *Science* **1996**, *274*, 1726.
(42) Szebenyi, D. M. E.; Bilderback, D. H.; LeGrand, A.; Moffat, K.; Schildkamp, W.; Temple, B. S.; Teng, T. *J. Appl. Crystallogr.* **1992**, *25*, 414.
(43) *Philos. Trans. R. Soc. London A* **1992**, *340*, 167 (Cruickshank, D. W. J., Helliwell, J. R., Johnson, L. N., Eds).
(44) Leemans, W. P.; Schoenlein, R. W.; Volfbeyn, P.; Chin, A. H.; Glover, T. E.; Balling, P.; Zolotorev, M.; Kim, K. J.; Chattopadhyay, S.; Shank, C. V. *Phys. Rev. Lett.* **1996**, *77*, 4182.
(45) Schoenlein, R. W.; Chin, A. H.; Glover, T. E.; Shank, C. V.; Leemans, W. P.; Volfbeyn, P.; Kim, K.-J.; Chattopadhyay, S. In *Ultrafast Phenomena X*; Fujimoto, J., Zinth, W., Barbara, P. F., Knox, W. H., Eds.; Springer-Verlag: Berlin, 1996; Vol. 62, p 122.
(46) Schoenlein, R. W.; Leemans, W. P.; Chin, A. H.; Volfbeyn, P.; Glover, T. E.; Balling, P.; Zolotorev, M.; Kim, K.-J.; Chattopadhyay, S.; Shank, C. V. *Science* **1966**, *274*, 236.
(47) Lin, S. H.; Chao, C. H.; Ma, H.; Rentzepis, P. M. In *Time-Resolved Electron and X-ray Diffraction*, Rentzepis, P. M., Ed. *Proc. SPIE-Int. Soc. Opt. Eng.* **1995**, *2521*, p 258.
(48) Barty, C. P. J.; Ben-Nun, M.; Guo, T.; Ráksi, F.; Rose-Petruck, C.; Squier, J.; Wilson, K. R.; Yakovlev, V. V.; Weber, P. M.; Jiang, Z.; Ikhlef, A.; Kieffer, J.-C. In *Time-Resolved Electron and X-ray Diffraction*; Rentzepis, P. M., Helliwell, J., Eds.; Oxford University Press: New York, in press.
(49) Ben-Nun, M.; Martinez, T. J.; Weber, P. M.; Wilson, K. R. *Chem. Phys. Lett.* **1996**, *262*, 405.
(50) Debye, P.; Bewilogua, L.; Ehrhardt, F. *Phys. Z.* **1929**, *30*, 84.
(51) Ischenko, A. A.; Golubkov, V. V.; Spiridonov, V. P.; Zgurskii, A. V.; Akhmanov, A. S.; Vabischevich, M. G. *Appl. Phys. B* **1983**, *32*, 161.
(52) Ischenko, A. A.; Golubkov, V. V.; Spiridonov, V. P.; Zgurskii, A. V.; Akhmanov, A. S.; Vabischevich, M. G. *Vest. Mosk. University Khim.* **1985**, *25*, 385.
(53) Rood, A. P.; Milledge, J. *J. Chem. Soc., Faraday Trans. 2* **1984**, *9*, 1145.
(54) Ischenko, A. A.; Spiridonov, V. P.; Ewbank, J. D. *J. Mol. Struct.* **1993**, *300*, 115.
(55) Ischenko, A. A.; Ewbank, J. D.; Schafer, L. *J. Mol. Struct.* **1994**, *320*, 147.
(56) Ewbank, J. D.; Schafer, L.; Ischenko, A. A. *J. Mol. Struct.* **1994**, *321*, 265.
(57) Ischenko, A. A.; Schafer, L.; Ewbank, J. D. *J. Mol. Struct.* **1996**, *376*, 157.
(58) Williamson, J. C.; Dantus, M.; Kim, S. B.; Zewail, A. H. *Chem. Phys. Lett.* **1992**, *196*, 529.
(59) Williamson, J. C.; Cao, J.; Ihee, H.; Frey, H.; Zewail, A. H. *Nature* **1997**, *386*, 159.
(60) Mourou, G. A.; Williamson, S. *Appl. Phys. Lett.* **1982**, *41*, 44.
(61) Williamson, S.; Mourou, G.; Li, J. C. M. *Phys. Rev. Lett.* **1984**, *52*, 2364.
(62) Elsayed-Ali, H. E.; Herman, J. W. *Appl. Phys. Lett.* **1990**, *57*, 1508.
(63) Herman, J. W.; Elsayed-Ali, H. E. *Phys. Rev. Lett.* **1992**, *68*, 2952.
(64) Herman, J. W.; Elsayed-Ali, H. E. *Phys. Rev. Lett.* **1992**, *69*, 1228.
(65) Herman, J. W.; Elsayed-Ali, H. E.; Murphy, E. A. *Phys. Rev. Lett.* **1993**, *71*, 400.
(66) Herman, J. W.; Elsayed-Ali, H. E. *Phys. Rev. B* **1994**, *49*, 4886.
(67) Aeschlimann, M.; Hull, E.; Schmuttenmaer, C. A.; Cao, J.; Gao, Y.; Mantell, D. A.; Elsayed-Ali, H. E. In *Time-Resolved Electron and X-ray Diffraction*; Rentzepis, P. M., Ed. *Proc. SPIE-Int. Soc. Opt. Eng.* **1995**, *2521*, 103.
(68) Elsayed-Ali, H. E.; Weber, P. M. In *Time-Resolved Electron and X-ray Diffraction;* Rentzepis, P. M., Helliwell, J., Eds.; Oxford University Press: New York, in press.
(69) Williamson, J. C.; Zewail, A. H. *Proc. Natl. Acad. Sci. U.S.A.* **1991**, *88*, 461.
(70) Williamson, J. C.; Zewail, A. H. *J. Phys. Chem.* **1994**, *98*, 2766.
(71) Ischenko, A. A.; Ewbank, J. D.; Schafer, L. *J. Phys. Chem.* **1994**, *98*, 4287.
(72) Ischenko, A. A.; Ewbank, J. D.; Schafer, L. *J. Phys. Chem.* **1995**, *99*, 15790.
(73) Ischenko, A. A.; Lobastov, V. A.; Schafer, L.; Ewbank, J. D. *J. Mol. Struct.* **1996**, *377*, 261.
(74) Martinez, T. J.; Ben-Nun, M.; Levine, R. D. *J. Phys. Chem.* **1996**, *100*, 7884.
(75) Martínez, T. J.; Ben-Nun, M.; Levine, R. D. *J. Phys. Chem.* **1997**, *101*, 6389.
(76) Volkmer, M.; Meiier, C.; Lieschke, J.; Mihill, A.; Fink, M.; Bowering, N. *Phys. Rev. A* **1996**, *53*, 1457.
(77) Volkmer, M.; Meir, C.; Mihill, A.; Fink, M.; Bowering, N. *Phys. Rev. Lett.* **1996**, *68*, 2289.
(78) Azaroff, L. V.; Kaplow, R.; Kato, N.; Weiss, R. J.; Wilson, A. J. C.; Young, R. A. *X-ray Diffraction*; McGraw-Hill: New York, 1974.
(79) Messiah, A. *Quantum Mechanics*; North-Holland Publishing Co.: Amsterdam, 1967.
(80) Shibata, S.; Hirota, F. In *Stereochemical Applications of Gas-Phase Electron Diffraction;* Hargittai, I., Hargittai, M., Eds.; VCH: New York, 1988.
(81) Mott, N. F.; Massey, H. S. *The Theory of Atomic Collisions*; Clarendon Press: Oxford, U.K., 1971.
(82) *Time Dependent Quantum Molecular Dynamics*; NATO ASI Series; Broeckhove, J., Lathouwers, L., Eds.; Plenum: New York, 1992.
(83) Seideman, T. *J. Chem. Phys.* **1995**, *103*, 7887.
(84) Herzberg, G. *Molecular Spectra and Molecular Structure I. Spectra of Diatomic Molecules*; Van Nostrand: Princeton, NJ, 1967.
(85) Rose, M. E. *Elementary Theory of Angular Momentum*; John Wiley & Sons: New York, 1957.
(86) Allen, H. C., Jr.; Cross, P. C. *Molecular Vib-Rotors*; John Wiley & Sons: New York, 1963.
(87) Zare, R. N. *Angular Momentum*; John Wiley & Sons: New York, 1988.
(88) Kosloff, R. *Annu. Rev. Phys. Chem.* **1994**, *45*, 145.
(89) Felker, P. M.; Baskin, J. S.; Zewail, A. H. *J. Phys. Chem.* **1986**, *90*, 724.
(90) Le Roy, R. J.; McDonald, R. G.; Burns, G. *J. Chem. Phys.* **1976**, *65*, 1485.
(91) Dantus, M.; Kim, S. B.; Williamson, J. C.; Zewail, A. H. *J. Phys. Chem.* **1994**, *98*, 2782.
(92) Gruebele, M.; Zewail, A. H. *J. Chem. Phys.* **1993**, *98*, 883.
(93) Fischer, I.; Villeneuve, D. M.; Vrakking, M. J. J.; Stolow, A. *J. Chem. Phys.* **1995**, *102*, 5566.
(94) Kohler, B.; Yakovlev, V. V.; Che, J.; Krause, J. L.; Messina, M.; Wilson, K. R.; Schwentner, N.; Whitnell, R. M.; Yan, Y. *Phys. Rev. Lett.* **1995**, *74*, 3360.
(95) Liu, Q.; Wan, C.; Zewail, A. H. *J. Chem. Phys.* **1996**, *105*, 5294.
(96) Tellinghuisen, J. *J. Chem. Phys.* **1985**, *82*, 4012.
(97) Arfken, G. *Mathematical Methods for Physicists*; Academic Press: Boston, MA, 1985.